COBALT DOPING OF SEMICONDUCTING BORON CARBIDE USING COBALTOCENE

THESIS

Lonnie Carlson, Major, USA
AFIT/GNE/ENP/07-01

DEPARTMENT OF THE AIR FORCE
AIR UNIVERSITY

AIR FORCE INSTITUTE OF TECHNOLOGY

Wright-Patterson Air Force Base, Ohio

AFIT/GNE/ENP/07-01

COBALT DOPING OF SEMICONDUCTING BORON CARBIDE USING COBALTOCENE

THESIS

Presented to the Faculty

Department of Engineering Physics

Graduate School of Engineering and Management

Air Force Institute of Technology

Air University

Air Education and Training Command

In Partial Fulfillment of the Requirements for the

Degree of Master of Science in Nuclear Engineering

Lonnie Carlson, BS

Major, USA

March 2007

AFIT/GNE/ENP/07-01

COBALT DOPING OF SEMICONDUCTING BORON CARBIDE USING COBALTOCENE

Lonnie Carlson, BS
Major, USA

Approved:

David A. LaGraffe David LaGraffe, LTC, USA (Chairman)	6 Mar 07 Date
Robert L Hengehold Robert L. Hengehold (Member)	12 Mar 07 Date
Jennifer L. Brand Jennifer J. Brand (Member)	16 Feb 07 Date

AFIT/GNE/ENP/07-01

Abstract

The decomposition of cobaltocene and metacarborane (*closo*-1,7-dicarba-decaborane) under low energy electron irradiation at about 200 K results in a material with the Fermi level closer to the valence band than the material resulting from the decomposition of metacarborane alone. This indicates that cobaltocene provides a relatively p-type dopant as seen in ultraviolet photoemission spectroscopy/inverse photoemission spectroscopy. Upon warming to room temperature, however, the Fermi level shifts towards the conduction band, suggesting an n-type dopant. This temperature dependent surface photovoltage effect is not compelling evidence for the majority carrier type but does suggest an increase in the carrier concentration in semiconducting boron carbides with cobaltocene fragment doping.

Using cobaltocene to introduce dopants into a orthocarborane (*closo*-1,2-dicarbadecaborane) derived film, deposited by plasma enhanced chemical vapor deposition, a semiconducting boron carbide homojunction diode has been fabricated. This diode has potential applications in neutron detection, direct neutron power conversion, and as a dilute magnetic semiconductor.

Acknowledgements

I would like to express my sincere appreciation to my faculty advisor, LTC David LaGraffe, for giving me the latitude and resources to run with this experiment, for knowing when to apply the boot, and for knowing when to leave me alone.

Drs. Jennifer Brand and Peter Dowben ensured my success by providing outstanding resource support, excellent direction and guidance, and just enough cheerleading and mentoring to keep me from breaking things when all was not well.

Drs. Neil Boag and Ildar Sabirianov were extremely helpful in helping me learn how to use, diagnose, and fix the plasma reactor needed to fabricate diodes. I would still be fixing vacuum problems without their help.

Snjezana "Snow" Balaz spent many late nights helping me get photoemission/ inverse photoemission data that was critical to many of the key results presented in this thesis.

I would also like to express my appreciation to Dr. Robert Hengehold for taking time away from his busy schedule as the Engineering Physics department head to sit on my committee.

Foremost, I want to offer my utmost gratitude to my family. My wife and kids did a great job surviving with me being gone for nearly three months. I love you all and cannot express the appreciation I have for you allowing me to choose a challenging research topic that would keep me away from home.

Lonnie Carlson

Table of Contents

Page

List of Figures

Figure Page

Figure Page

List of Tables

COBALT DOPING OF SEMICONDUCTING BORON CARBIDE USING COBALTOCENE

1. Introduction

This thesis presents the results of two different methods of doping semiconducting boron carbide films with cobalt, using cobaltocene as the cobalt source. The first method involves adsorption and decomposition of a boron carbide source compound and cobaltocene in ultra high vacuum conditions and observing changes in the energy band structure after electron beam decomposition. The second method is the fabrication of a diode using plasma enhanced chemical vapor deposition (PECVD) of a carborane (boron carbide) source compound and cobaltocene.

1.1. Motivation

Boron carbide semiconductors have several potentially promising nuclear engineering related uses. Boron carbide is easily deposited, chemically stable, and mechanically strong. Semiconductors made from boron carbide would likely be resistant to corrosive, high temperature, and mechanically abrasive environments. [1] Because ^{10}B has a large thermal neutron capture cross section (3840 barns) and results in the following reactions:

$$^{10}B + n \rightarrow {}^{7}Li(0.84\ MeV) + \alpha(1.47\ MeV) + \gamma\ (0.48\ MeV)\ (94\%)$$

$$^{10}B + n \rightarrow {}^{7}Li(1.02\ MeV) + \alpha(1.78\ MeV)\ (\sim 6\%) \qquad (1.1)$$

boron carbide diodes could potentially be used as neutron detectors [1,2] as shown in Figure 1-1 as well as in other nuclear applications such as neutron direct power conversion. [3]

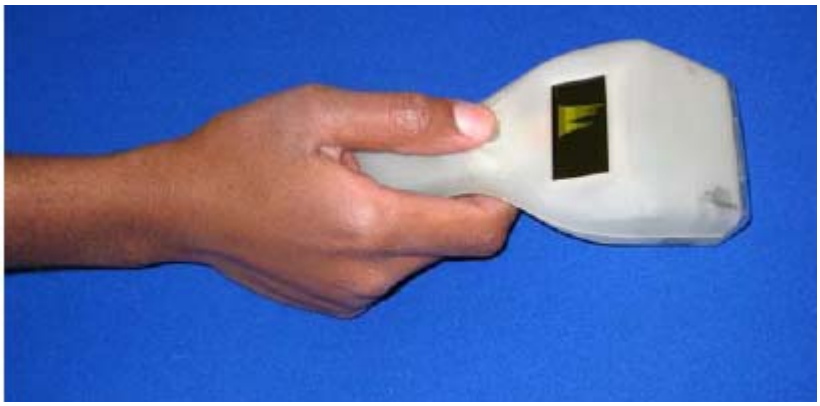

Figure 1-1. Prototype handheld neutron detector fabricated at the University of Nebraska-Lincoln.

Boron carbide p-n junction diodes have previously been fabricated using both doped silicon substrates as one side of the junction, as well as all boron carbide devices grown on metal substrates. There have also been successful attempts at n-type doping of boron carbide using several of the transition metals but no successful p-type dopant has been found. [1-4] There are indications that cobalt may act as a p-type dopant which could allow for significantly better performing p-n junction diodes and more successful applications. [5]

A potential application for boron carbide semiconductors is in nuclear reactor monitoring. The large neutron capture cross section, ruggedness, and low cost of a boron carbide semiconductor would be ideal for use as a current-mode neutron detector to monitor the real-time neutron flux in a reactor.

Another potential commercial application of boron carbide semiconductors is use in direct power conversion. As shown in equation (1.1), neutron absorption in ^{10}B results in production of an α particle. This α particle loses its energy very rapidly in the boron carbide semiconductor resulting in millions of electron-hole pairs generated. These charge carriers are separated by the electric field in the diode resulting in substantial current flow and power generated. The process is similar to that of a solar cell except that a solar cell only generates one electron per photon compared to the millions of electrons resulting from each neutron absorption. The neutrons that escape a nuclear reactor core do not contribute to power generation and must be stopped with shielding. This shielding requires a large volume of material which increases reactor size and cost and can become radioactive as impurities become activated by neutron capture. Using boron carbide semiconductors along the reactor periphery would allow conversion of the normally lost leakage neutron energy into power while also considerably reducing the required neutron shielding. Direct power conversion could potentially also be used to build higher efficiency nuclear power sources for applications currently using radio-isotope thermoelectric generators (RTG).

Cobalt doped boron carbide semiconductors may also have potential uses in the emerging field of spintronics and dilute magnetic semiconductors. Current semi-conductors use the charge on the electron as an information carrier while magnetic data storage devices rely on electron spin. Controlling the electron spin in a dilute magnetic semiconductor increases the amount of information that can be carried and breaks down the barrier between the two types of devices. Cobalt, a ferromagnetic material, may

provide the desired room temperature ferromagnetism needed for many dilute magnetic semiconductor applications.

The Defense Threat Reduction Agency (DTRA) and other United States Government agencies continually seek tools to assist their mission of nuclear deterrence as well as nuclear weapon treaty monitoring. One critical area of research is the development of portable, accurate tools for detecting and identifying special nuclear materials (SNM) such as uranium-235 or plutonium-239, which make up nuclear weapon fuels.

During natural radioactive decay, uranium or plutonium emit alpha particles and gamma rays. These SNM also spontaneously fission into two fission fragments and typically release 2-3 neutrons and several gamma rays. Because there is nearly zero neutron background and a large gamma background, it is much easier to distinguish the large relative change in number of neutrons due to the presence of SNM than it is the relatively small change in gammas. Radioactive materials emit gamma rays of specific energies and it is possible to determine the type of material by measuring those energies under controlled conditions. Unfortunately, the passage of the gamma rays through the SNM fuel, weapon assembly, and storage containers causes the majority of the emitted gamma rays to change energy and lose the information that can specifically identify the type of material. Because the neutron background is so small, the presence of neutrons is a good indicator of fissile materials and less likely to lead to "false positive" identification then relying on gamma detection only. The detection of SNM ideally occurs at the point of origin where the material is transported for shipping. Detection certainly must occur no later than at the point of entry into the U.S. A low cost, portable

neutron detector would greatly increase the probability of detection, which is currently close to nil, of SNM before entry into the country.

DTRA is also involved in verifying nuclear weapon treaty compliance. This process is currently conducted using gamma ray detection and spectroscopy of the unopened weapon system. This system is easy to spoof however as any number of other radioactive sources could be used to replicate a missing fuel assembly. Neutrons are much more difficult to spoof and would provide a much more reliable verification method.

1.2. Background

It is desirable to have semiconductor devices that can operate in high temperature or harsh environments. Boron carbide is a hard, corrosion-resistant, refractory material. [1,4] It is one of the hardest materials in existence and has a high melting temperature of 2350°C. Its high modulus of elasticity, low density, good thermal and electric properties as well as a large thermal neutron capture cross section (3840 barns for ^{10}B and 752 barns for natural boron) and chemical inertness make boron carbide a candidate for use as a neutron detecting semiconductor. Boron carbide semiconductors have been desired since the 1950's but devices fabricated using sintering or hot pressing typically had too low resistivity to be useful. [6] Only in about the last ten years has progress been made in controlling fabrication and optimizing physical properties by using chemical vapor deposition techniques. Boron carbide is a stable single phase compound typically with 8-20% atomic percent carbon concentrations. The most stable structure, B_4C, is rhombohedral with icosahedral clusters at the vertices as shown in Figure 1-1. The boron

and carbon atoms making up the icosahedra can replace each other which explains the wide range of carbon concentrations. [6]

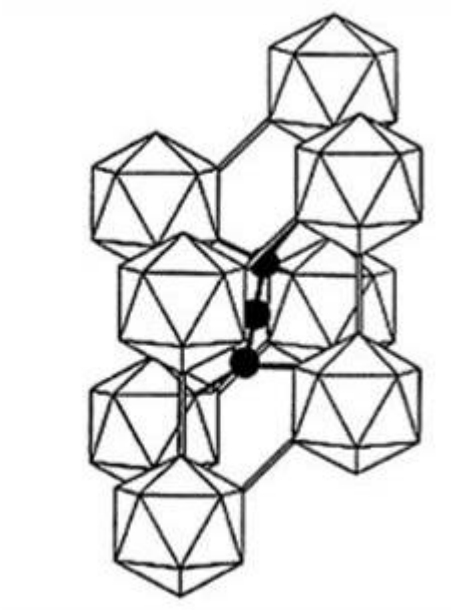

Figure 1-2. The rhombohedral crystal structure of boron carbides showing atoms placed at the icosahedra vertices within the three-atom intericosahedral chain. [5]

The semiconducting form of boron carbide is naturally a p-type material at high temperatures and carbon concentrations. [5,7] Because it is desirable in device fabrication to be able to change the semiconductor material from p-type to n-type or increase the p-type doping level, there have been several attempts to dope boron carbide with the transition metals or Group III, IV, or V elements. Various potential dopants such as mercury, zirconium, and phosphorus have failed to dope boron carbide due to problems such as clustering of the dopant.[4,8,9] The majority of the transition metals (V, Cr, Mn, Fe, Ni) have successfully doped boron carbide to n-type but there is a lack of p-type dopants. [5],10] There are indications, however, that copper and cobalt may act as p-type dopants in boron rich materials. [5]

Cobalt has several potentially useful properties as part of a boron carbide semiconductor besides the potential to act as a p-type dopant. Cobalt is ferromagnetic with a high Curie temperature of 1388 K which could potentially lead to dilute magnetic semiconductors with a magnetically adjustable band gap. Cobalt is also a hard metal with good oxidation resistance that could lead to even more rugged boron carbide semiconductors that can operate in high temperature, corrosive, and mechanically abrasive environments. The stable isotope of cobalt is ^{59}Co. When ^{59}Co is exposed to neutrons, neutron capture results in ^{60}Co which is a strong gamma emitter. The use of cobalt doped boron carbides as neutron detectors must be balanced against the resulting gamma ray emission if practical applications are to be built.

Boron carbide has previously been successfully used as components of heterojunction diodes [11], homojunction diodes [4], and heteroisomeric diodes [3] as discussed further in chapter 2. An engineering approach is necessary however to develop and evaluate better semiconducting boron carbide diodes.

1.3. Problem Statement

Does cobalt, using cobaltocene as a source, dope semiconducting boron carbide?

1.4. Research Methodology

A two step method was used to determine if cobalt, introduced via cobaltocene, dopes semiconducting boron carbide. The source compounds and techniques will be discussed in more detail in later chapters. The first step involved adsorption under ultra high vacuum (10^{-9} Torr base pressure) of extremely thin layers of metacarborane ($C_2B_{10}H_{12}$) and cobaltocene ($Co(C_5H_5)_2$) on a clean gold substrate at low temperature

(~200 K). An electron beam dehydrogenated the metacarborane to create an involatile semiconducting boron carbide, and dissociated the cobaltocene molecule in order to deposit cobalt. The resulting films were then analyzed using photoemission spectroscopy and inverse photoemission spectroscopy (PES/IPES) to determine the changes to the energy band structure that can indicate doping type. X-ray photoemission spectroscopy (XPS) determined if cobalt bonds with atoms in the boron carbide icosahedral cage.

The second step involved the fabrication of a diode that displays the current-voltage response typical of a rectifying p-n junction diode. Preliminary information from the photoemission/inverse photoemission measurements indicated that the cobaltocene fragment doping of boron carbide was n-type, unlike the hypothesized p-type. This information led to attempting to fabricate the n-type side of the p-n junction diode by introducing orthocarborane and cobaltocene into a plasma enhanced chemical vapor deposition reactor in order to grow a thin doped film on a silver substrate. Orthocarborane was then introduced into the plasma, with no cobaltocene, to grow the p-type side of the p-n junction.

1.5. Preview

Introducing cobaltocene into orthocarborane, a p-type boron carbide source, during plasma enhanced chemical vapor deposition (PECVD) and then depositing only orthocarborane via PECVD resulted in a p-n junction. This indicates that at room temperature, cobalt appears to be an n-type dopant.

Interestingly, the photoemission spectroscopy and inverse photoemission spectroscopy (PES/IPES) studies at low temperature (~200 K) indicate that the cobalt acts as a

p-type dopant. Warming the sample to room temperature and repeating PES/IPES shows the Fermi level shifts closer to the conduction band, indicating a transition to a more n-type semiconductor material. This shift in doping type at different temperatures highlights that dopants of semiconducting boron carbide, such as nickel and iron, may act differently than the more conventional silicon and germanium dopants.

While speculative, it may be that electron carrier creation requires a larger activation energy than hole carriers, although many more electron carrier states may exist. In such a system, p-type carriers dominate at lower temperatures and n-type carriers dominate at higher temperatures. This model is, in fact, entirely consistent with the speculations about trapping states proposed by Werheit and coworkers. [5]

2. Theory

Semiconducting materials are essential to solid state devices. The p-n junction diode is a common electronic device fabricated by combining n-type and p-type semi-conducting regions. To understand the physical processes that occur when these materials are combined, it is necessary to be familiar with several concepts such as material properties, atomic bonding and bandgap energy, effects of impurities, and energy bands.

2.1. Electronic Band Theory.

The electrons in an atom have quantized energy levels but may interact in multiple ways with adjacent atoms. These possible interactions lead to a grouping together of possible energy states into a band structure. The schematic of a simple band diagram seen in Figure 2-1 [12] shows the conduction band, valence band, and bandgap (E_g) for an insulator, semiconductor, and a metal. The valence band consists of electrons in their valence state while the conduction band consists of unoccupied energy states. The bandgap is often referred to as the “forbidden gap” as, ideally, there are no available energy states that an electron can occupy. The difference in the energy between the highest occupied molecular orbital (HOMO) in the valence band and the lowest unoccupied molecular orbital (LUMO) in the conduction band is known as the bandgap energy. The bandgap energy is the minimum energy required for an electron in a valence state to move into the conduction band. For an electric current to flow through the solid, there must be empty states in the conduction or valence bands for electrons and holes to be able to move relatively freely through the solid. The bandgap of metals is

approximately 0 eV due to the overlap of the conduction and valence bands while insulator bandgaps are generally greater than 6 eV.

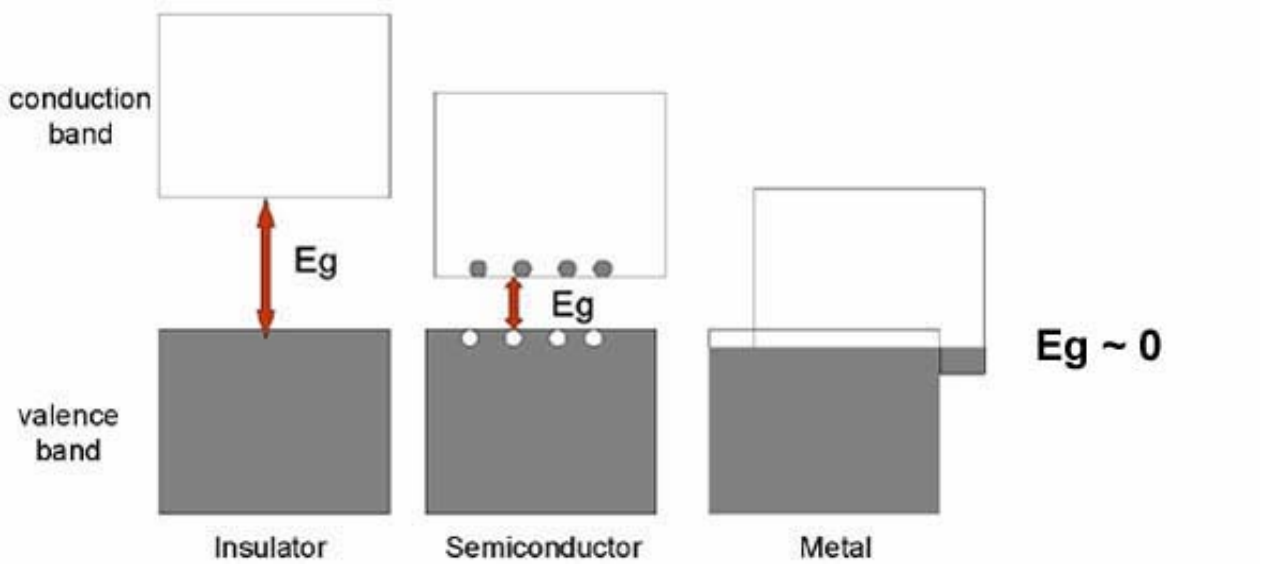

Figure 2-1. Schematic of simple band diagrams comparing the bandgap between the conduction and valence bands for insulators, semiconductors, and metals. [12]

A more accurate representation of the band structure requires the use of Fermi-Dirac statistics and knowledge of the density of states. Fermi-Dirac statistics describe the probability that an electron has an energy E at a temperature T [13] and is given by equation (2.1):

$$F(E) = \frac{1}{e^{(E-E_f)/kT} + 1} \tag{2.1}$$

where E is the electron energy level, E_f is the Fermi energy, k is Boltzmann's constant, and T is the temperature in degrees K. From equation (2.1), we see that the Fermi energy is the energy at which an electron has a 50% probability of occupying that energy state, if such a state exists.

The number of occupied states within a region of energy is given by equation (2-2):

$$N(E)dE = g(E)F(E)dE \tag{2-2}$$

where *N(E)* is the number of electron occupied energy states, *F(E)* is the Fermi-Dirac distribution fill probability, and *g(E)* is the density of states. The density of states *g(E)* for free electrons is given by [13]:

$$g(E) = \frac{(2m_{eff})^{3/2} E^{1/2}}{2\pi^2 \hbar^3} \tag{2-3}$$

where m_{eff} is the effective mass of the charge carrier and $\hbar$ is Planck's constant. The effective mass is experimentally determined by measuring the carrier response to an applied electric field. Equation (2-3) results from solving the Schrödinger wave equation for a free electron in a box. [13] The electrons in a semiconductor are not free but it has been found that for states near the gap, the electrons behave very much like free electrons. This assumption and the fact there must be zero states in the gap for an ideal semiconductor gives rise to separate solutions for *g(E)* as shown in equations (2-4) and (2-5) which are based on the effective masses of holes and electrons and where the energy E=0 is defined at the valence band. [14]

$$g_e(E) = \frac{1}{\pi^2 \hbar^3} (2m_e^{*3}(E - E_g))^{1/2} \tag{2-4}$$

$$g_h(E) = \frac{1}{\pi^2 \hbar^3} (-2m_h^{*3} E)^{1/2} \tag{2-5}$$

A hole is a fixed position positive ion where an excited electron has left an electron vacancy. Electrons from nearby atoms can then move relatively easily between the holes resulting in a current from hole conduction. The available density of states for a semiconductor is shown in Figure 2-2. [14] We can see that the density of states for both the conduction and valence bands approach zero at the band edges as we would expect approaching the "forbidden" gap. For an intrinsic semiconductor, the Fermi energy, E_g, is in the middle of the bandgap. The positioning of the Fermi level within the gap will vary for doped semiconductors and will be important to the analysis of whether cobalt dopes boron carbide.

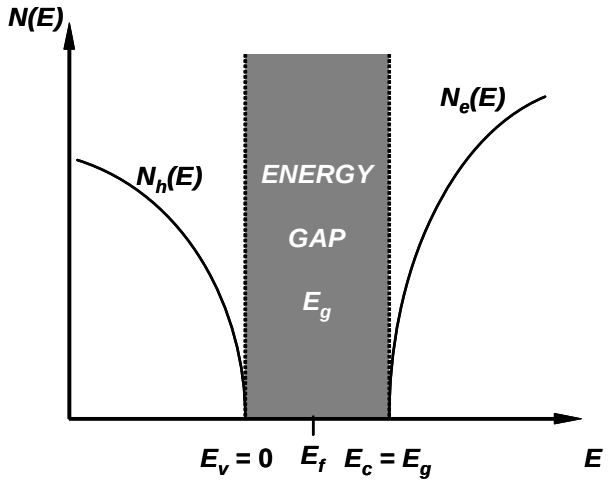

Figure 2-2. Example density of states for a semiconductor. The valence band edge is defined as the highest occupied molecular orbital (HOMO) while the conduction band edge it the lowest unoccupied molecular orbital (LUMO). For an intrinsic semiconductor, the Fermi energy, E_g, is in the middle of the bandgap. [14]

2.2. Intrinsic Semiconductor Material Properties.

Electronic materials are generally considered to be insulators, conductors or semiconductors as distinguished by their resistivity ρ (Ω·cm). Insulators such as diamond typically have very large resistivity, $\rho > 10^5$ Ω·cm. Conductors, such as most metals, have

a much lower resistivity, $\rho<10^{-3}$ Ω·cm and are very good at conducting electricity. Semiconductors, of which silicon (Si) is the most important, fill the middle ground and have the benefit that resistivity can be controlled through the addition of impurity atoms. [15] Metals are further distinguished by having a resistivity which increases with increasing temperature, while the resistivity of insulators and semiconductors decreases as the temperature increases.

Atoms in electronic materials bond together to form many types of crystals. The most important type of semiconductor crystal is the single crystal where the atoms form a highly ordered structure. An intrinsic semiconductor is one that has no impurities although this is impossible to achieve in practice. Compensated materials, with nearly equal holes and electron carriers, are often sought as a benchmark for the "intrinsic" material. Figure 2-3 [15] represents an intrinsic, two-dimensional group IVA lattice of a crystal with all covalent bonds filled.

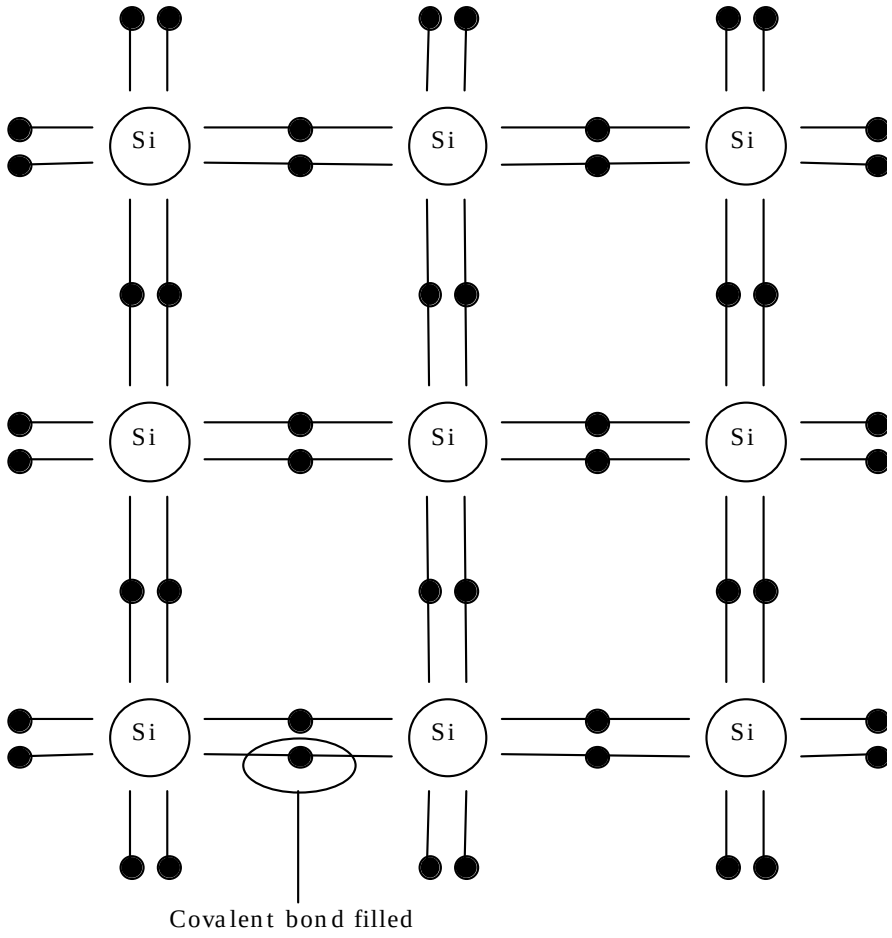

Figure 2-3. Two-dimensional lattice representation of Group IVA covalent bonds. At temperatures approaching 0 K, all covalent bonds are filled. [15]

As the temperature increases above 0 K in a semiconductor, an increasing number of electrons have energies along the high energy tail of the Maxwell-Boltzmann distribution and are energetic enough to overcome the bandgap and break their covalent bonds. This results in a hole and a conduction band electron as shown in Figure 2-4. [15]

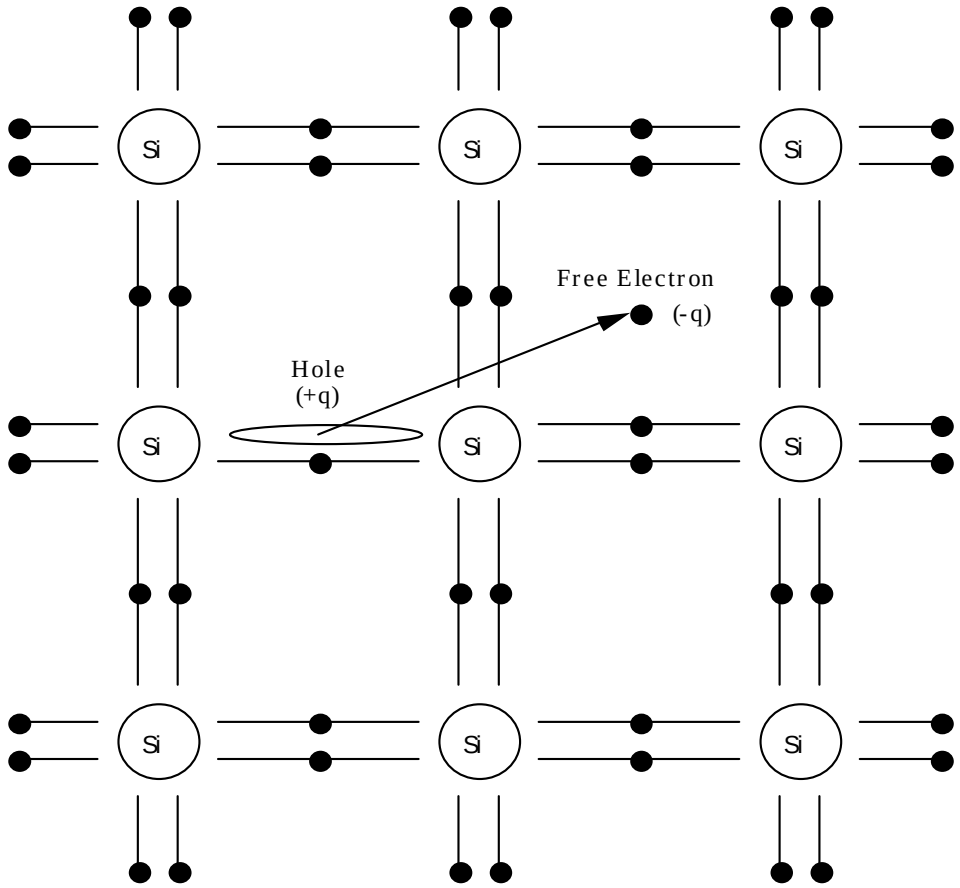

Figure 2-4. Breaking of covalent bonds above 0 K in a semiconductor due to increasing thermal energy of electrons results in a fixed hole and a free electron. [15]

The number of carriers available in an intrinsic semiconductor is very low at common temperatures as shown in Figure 2-5. [16] For Si at 300 K, only one in 10^{12} electrons has enough thermal energy to cross the bandgap and move into the conduction band so that a current may flow through the material. Doping the intrinsic material with impurities is a common technique to increase the number of carriers and reduce the resistivity of the material.

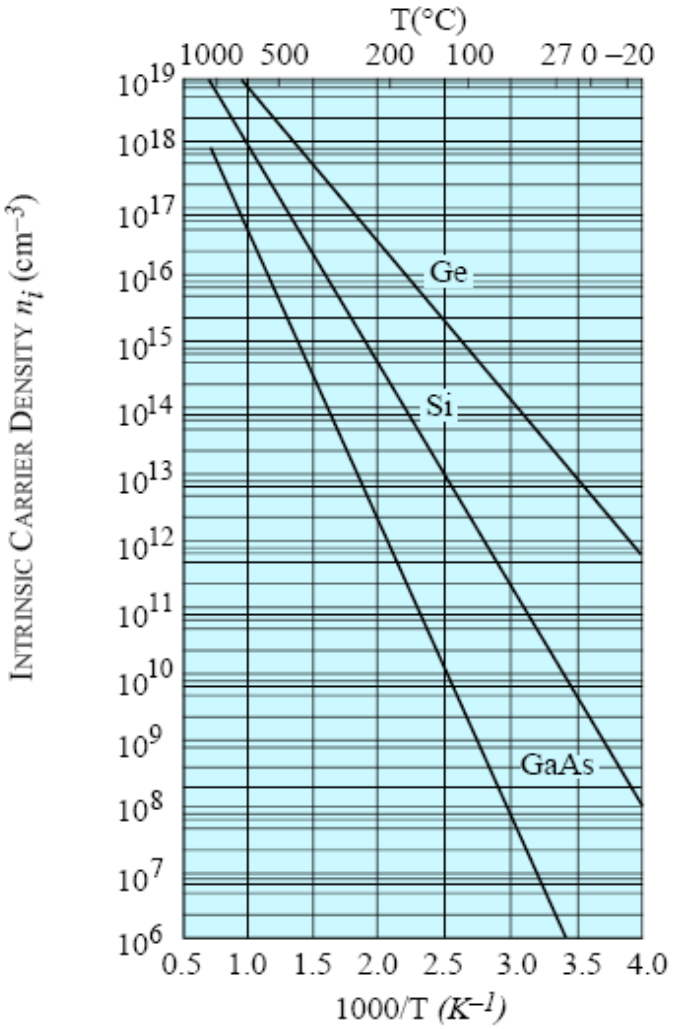

Figure 2-5. The intrinsic carrier density of three common semiconductors. At room temperature (~300 K) the carrier density of Si electrons in the conduction band is only ~10^{10} cm^{-3} out of an available 10^{22} cm^{-3}. [16]

2.3. Doped Semiconductor Material Properties.

All materials have some level of impurities in them such that the previously discussed intrinsic properties only provide a model of an ideal material. Doping semiconductor materials allows manipulation of the resistivity of the material and the hole and electron populations for specific applications. As previously shown, group IVA

materials such as carbon and silicon have a well ordered lattice. These group IVA atoms also have four of eight possible valence electrons in their outer shell and form covalent bonds with adjacent atoms to pair up all available electrons. Doping often consists of replacing a group IVA atom with a group IIIA or group VA atom. Group IIIA atoms such as boron, aluminum, and gallium have three valence electrons while group VA atoms such as phosphorus, nitrogen and arsenic have five. As shown in Figure 2-6 [15], when a group IIIA atom such as boron replaces a group IVA atom, an electron vacancy, or hole, exists and hole conduction can occur due to an available energy state. A group IIIA impurity in silicon or carbon is known as an "acceptor" impurity because of the impurity's ability to accept an electron and leave a mobile hole as the majority charge carrier. Doping with acceptor atoms results in a "p-type" semiconductor based on the positively charged hole majority carrier.

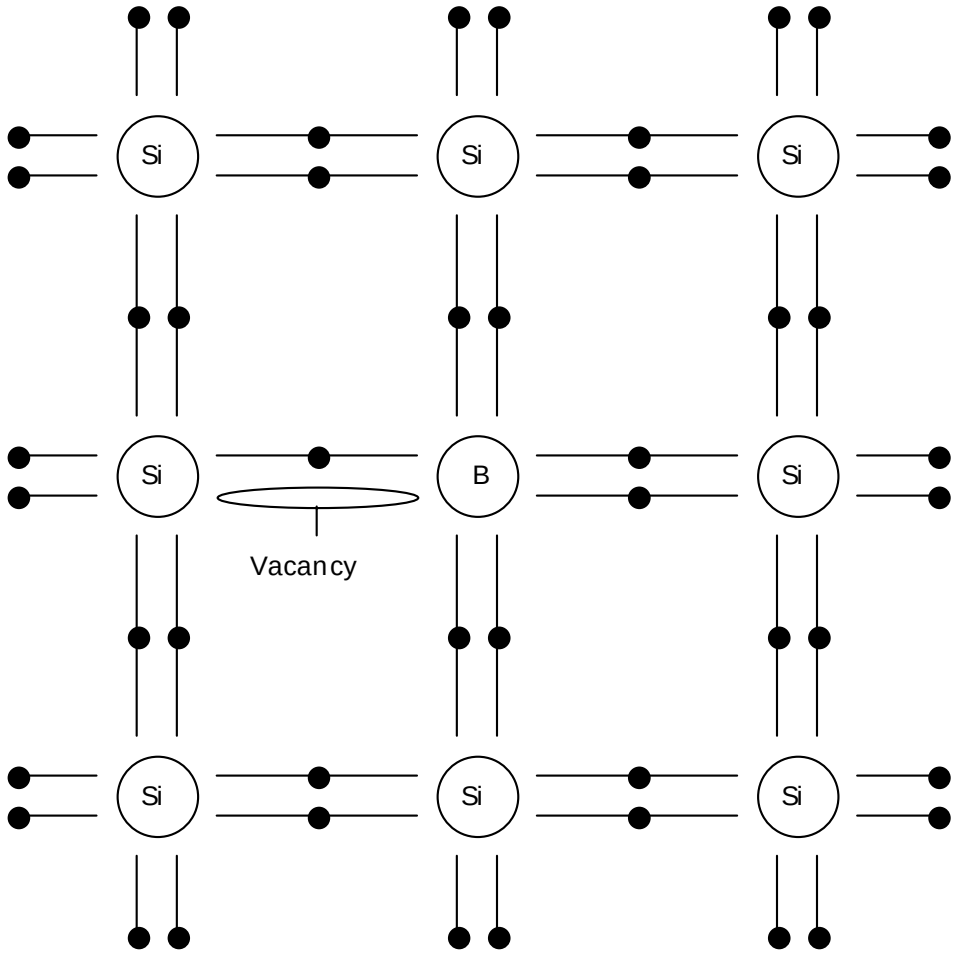

Figure 2-6. Schematic of p-type doping as a group IIIA atom (boron) replaces a group IVA atom in the lattice and leaves an electron vacancy which is modeled as a positively charged hole. [15]

When a semiconductor is doped p-type, the donor atom can introduce states in the bandgap and does drive the Fermi level closer to the valence band as shown in Figure 2-7. [16] Electrons from the valence band easily thermally ionize into the new states and leave a large number of corresponding holes available for conduction.

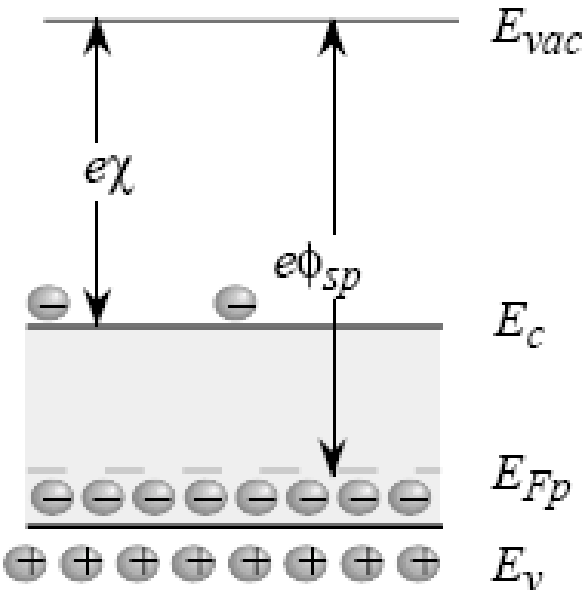

Figure 2-7. Introduction of energy states near the valence band by a p-type dopant pushes the Fermi level closer to the valence band. Electrons in the valence band are easily excited into the new fixed states which increases the number of mobile holes available for conduction in the valence band. [16]

A group VA impurity on the other hand has an extra valence electron that can not pair up with an electron from an adjacent group IVA atom as shown in Figure 2-8. [15] This electron is easily ionized from its atom and becomes part of the conduction band. Group VA impurities are known as donor atoms because they donate free electrons to the conduction band. These electrons become the majority carrier in this "n-type" semiconductor.

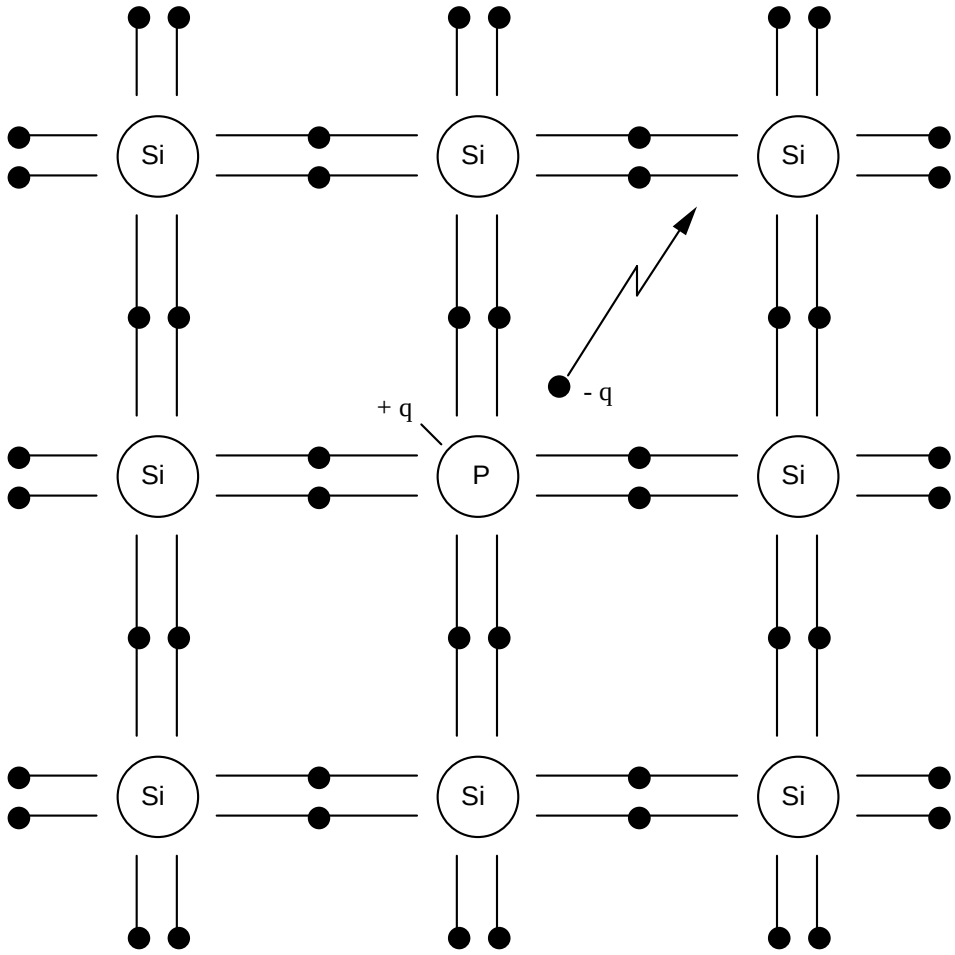

Figure 2-8. Schematic of n-type doping as a group VA atom (phosphorus) replaces a group IVA atom in the lattice resulting in an excess electron which may move into the conduction band. [16]

Doping n-type results in any new states in the gap being located near the conduction band as shown in Figure 2-9. [16] The Fermi level then shifts towards the conduction band. Electrons in atoms occupying these new states may then easily thermally excite into the conduction band and become the majority charge carriers.

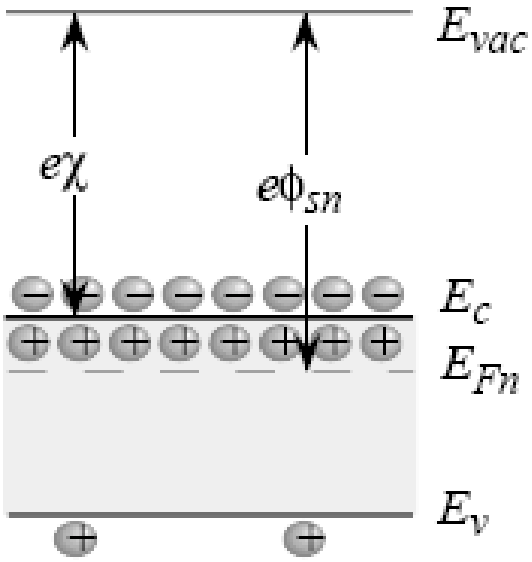

Figure 2-9. Introduction of energy states near the conduction band by a n-type dopant pushes the Fermi level closer to the conduction band. [16]

The temperature dependence of carrier concentration for a typical doped semiconductor is dependent upon the activation (ionization) energies of both the intrinsic material and the dopant as shown in Figure 2-10. [17] As the temperature increases from 0 K, the dopant impurities ionize first ("freeze out region") as the energy to the next available state is much smaller than the intrinsic material bandgap. Once all the impurity atoms have ionized, the carrier density remains essentially constant ("extrinsic region") because so few intrinsic atom electrons can ionize across the bandgap. Once the temperature is high enough for a substantial number of intrinsic atoms to ionize, the intrinsic carriers dominate as shown in the "intrinsic region". This temperature dependent carrier concentration also makes the resistivity of the material temperature dependent.

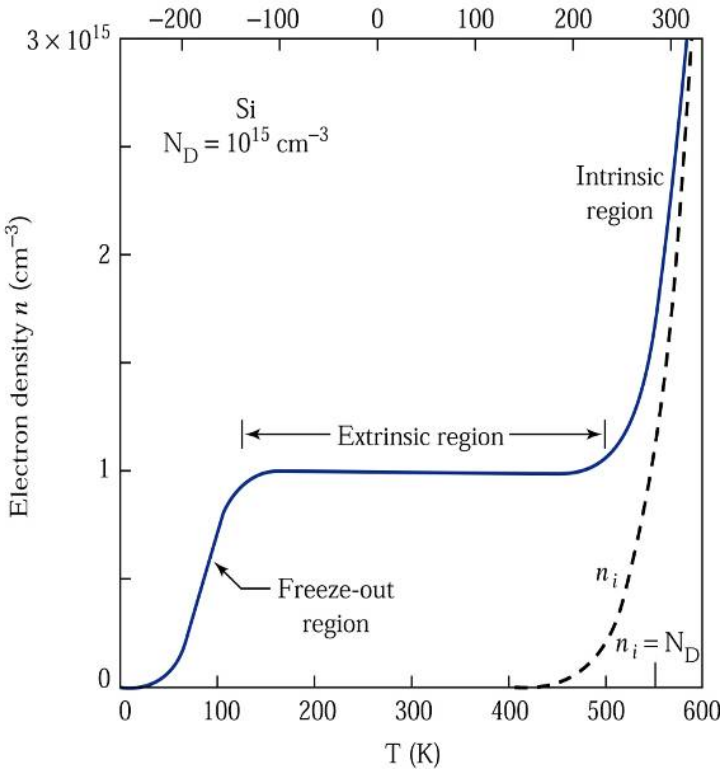

Figure 2-10. Temperature dependence of conduction band electron density for n-type Si. At low temperatures (<150 K), the carriers are dependent upon the thermal energy of the electrons in the states near the valence band. At T>150 K, all the excess electrons from the donor impurities are excited while very few of the intrinsic Si atoms ionize resulting in a saturation level. At T>500 K, excited electrons from the Si atoms begin to dominate the overall electron density. [17]

2.4. P-N Junction Diodes

The p-n junction formed by mating a p-type and an n-type semiconductor is critical to many semiconducting devices. There are two key principles that occur in a p-n junction. The first is that the Fermi energies are approximately at the donor level for n-type materials and the acceptor level for p-type materials. [13] Second, when two materials are placed together, thermodynamic equilibrium requires charge to transfer until the Fermi energies equalize in both materials. As shown in Figure 2-11 [16], the mobile holes from the p-type material diffuse to the n-type which has a much lower hole

concentration. Similarly, the majority electrons from the n-type diffuse to the p-type side. The remaining fixed charges generate an electric field that creates a drift current in opposition to the diffusion current. An unbiased p-n junction will reach an equilibrium point where the drift and diffusion currents exactly balance out leaving a "depletion region" with no mobile carriers.

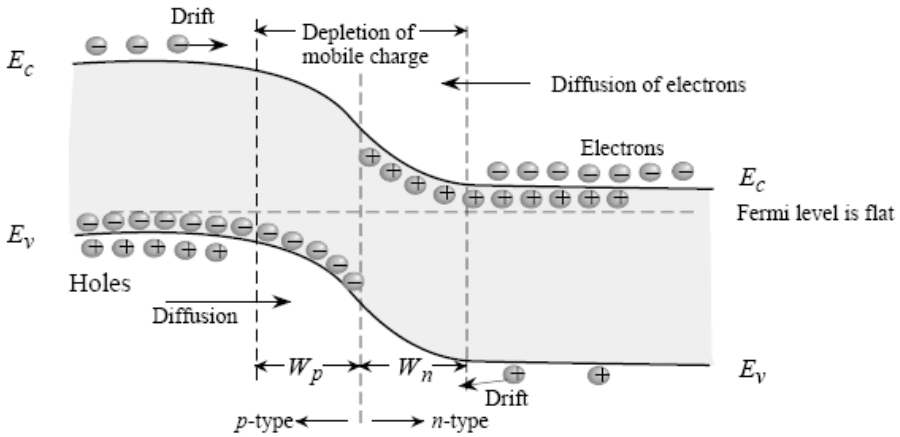

Figure 2-11. Mating of p- and n-type materials in an unbiased p-n junction results in the bands bending until the Fermi level is equal on both sides of the junction. The mobile majority carrier on each side of the junction diffuses to the other side until the generated electric field causes a drift current that exactly counterbalances the diffusion current. [16]

The ideal p-n junction has the important property that rectification occurs due to the junction only conducting under forward bias. Forward bias is defined as a positive voltage applied to the p-type side of the junction. A nearly ideal, real diode has the characteristics of exponential current growth under forward bias, with linear, nearly zero current under reverse bias as shown in Figure 2-12. [17] Breakdown under reverse bias typically occurs when the electric field is greater than 10^6 V/m. [17] The kinetic energy of electrons in the conduction band at breakdown is so great that they ionize additional

electrons from atoms as they traverse the lattice resulting in an “avalanche” of electrons and large current increases.

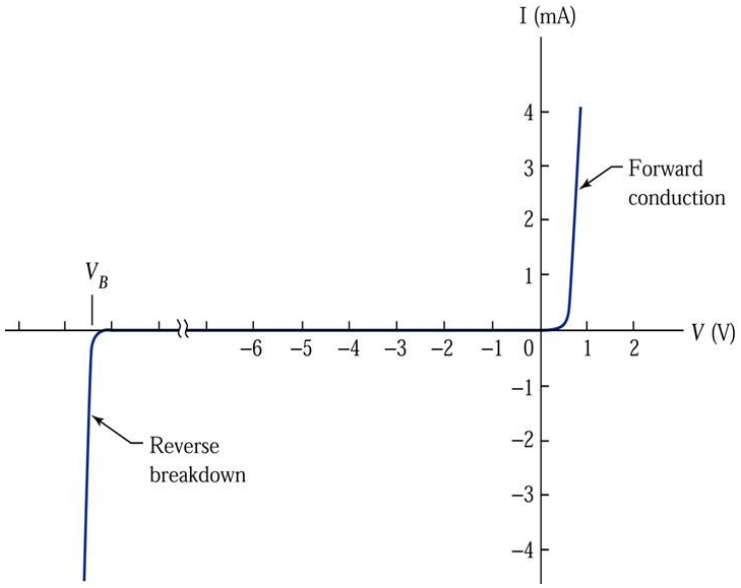

Figure 2-12. Current-Voltage (I-V) characteristics of a nearly ideal, real p-n junction diode where forward bias occurs for $V_D>0$. Current growth is exponential under forward bias and nearly zero and linear under reverse bias. “Avalanche” breakdown occurs under large reverse bias when electrons have enough kinetic energy to ionize additional electrons as they move through the material. [17]

When there is no bias on the p-n junction, a built in potential is created when mobile carriers diffuse across the junction and leave fixed, ionized atoms. The built in potential results from the electric field between these fixed charges and is equal to the energy level difference of a band on each side of the junction ($V_{bi} = E_{vp} – E_{vn}$). As shown in Figure 2-13, there is only a small fraction of the available density of states available for carriers to inject across the junction. [16]

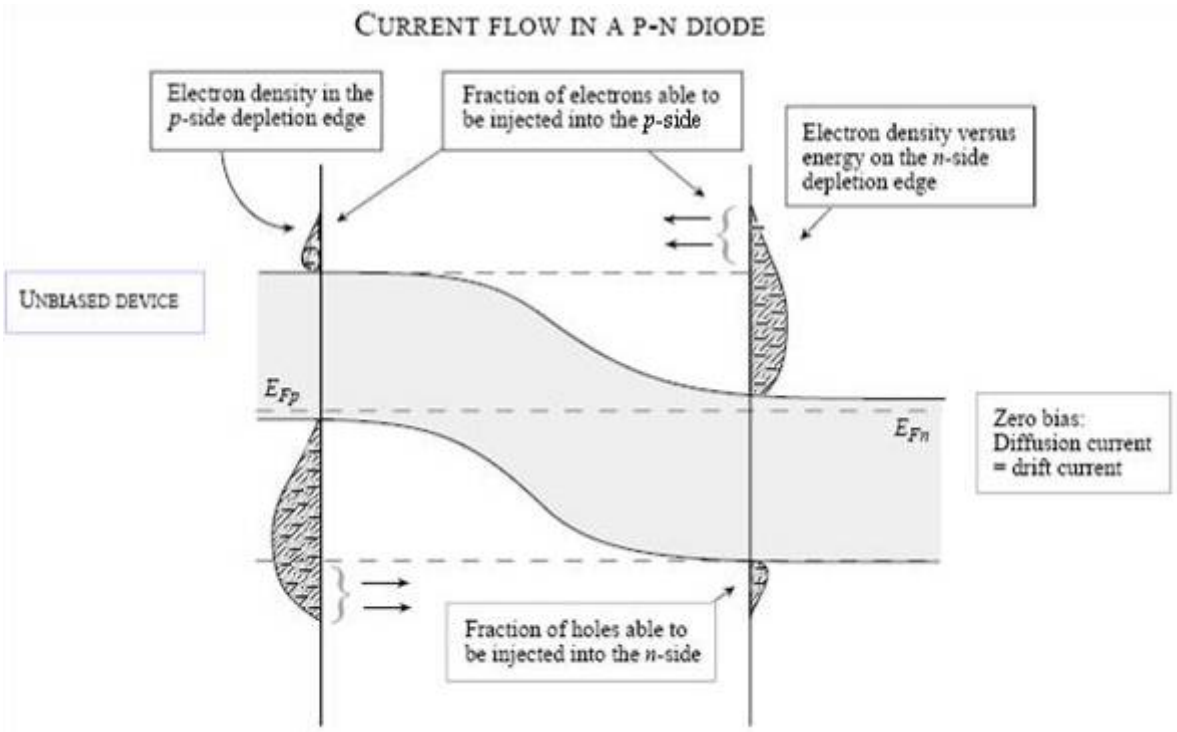

Figure 2-13. When a p-n junction is unbiased, the built in potential generates a drift current that offsets the diffusion current. The number of majority carrier holes and electrons available to inject across the junction is limited by the small overlap in the density of states. [16]

Under forward bias, the potential difference across the junction is reduced by the amount of the applied bias such that $V = V_{bi}-V_{applied}$. There is then an exponential increase in the carriers injected across the junction and the current flowing through the diode as shown in Figure 2-14. [16] Additionally, the depletion width decreases, which increases the likelihood of injection across the junction.

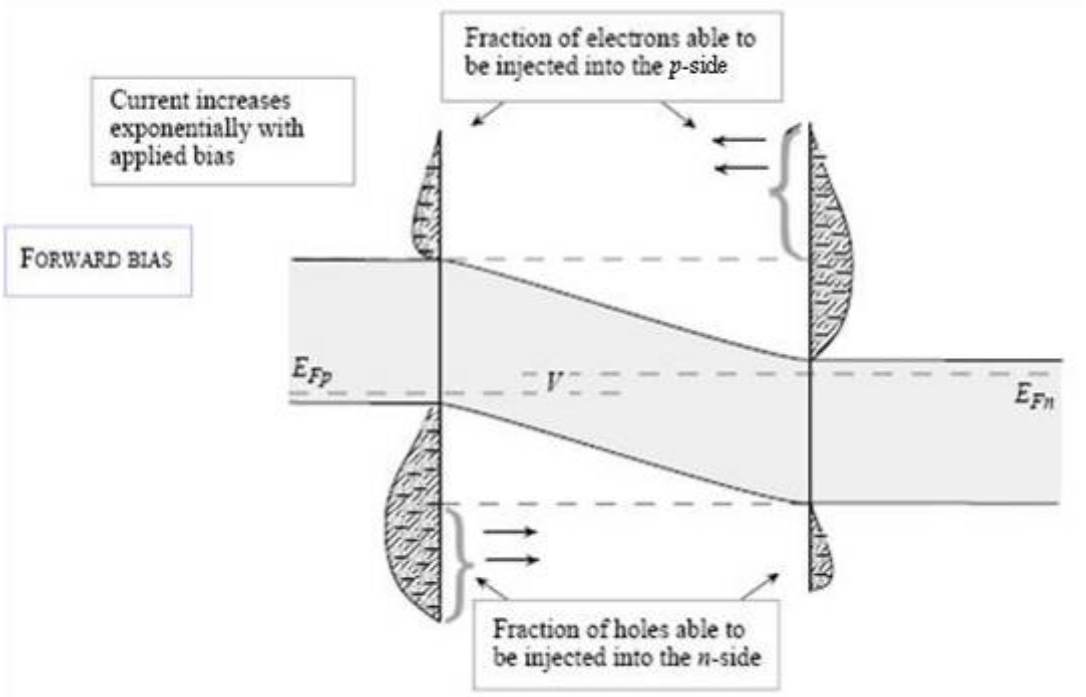

Figure 2-14. Under forward bias, the potential across the junction is decreased by the applied bias and a greater overlap of the density of states across the junction exponentially increases the injection of carriers and current. [16]

The current flow in an ideal reverse biased p-n junction is essentially zero due to the wider depletion region and negligible overlap of the density of states as shown in Figure 2-15. [16] Real diodes have a non-zero current due to carriers hopping between trap states within the gap or currents leaking across the diode surface.

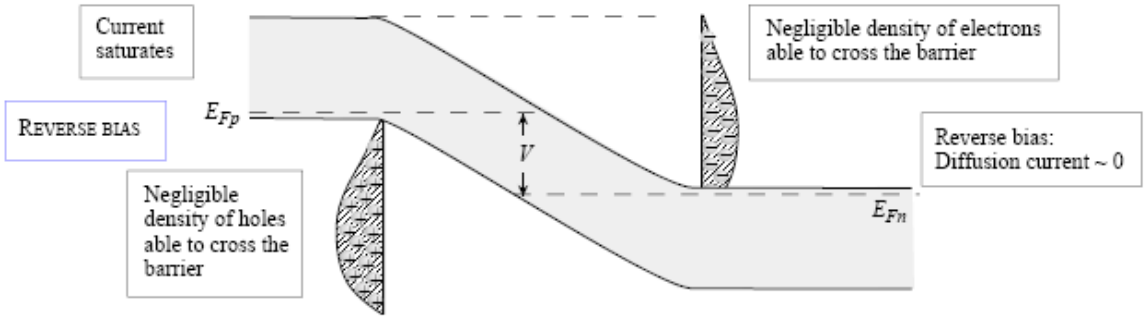

Figure 2-15. In an ideal reverse biased p-n junction the potential across the junction is increased by the amount of the applied bias and there is a negligible overlap of density of states so that the current is essentially zero. The depletion width also increases reducing the likelihood of injection. In reality, trap states within the gap allow increased current flow but still considerably less than the current under forward bias. [16]

2.5. Energy Band Spectroscopy

The density of states for the conduction and valence bands can be determined by using photoemission spectroscopy (PES) and inverse photoemission spectroscopy (IPES).

One type of PES is ultraviolet photoemission spectroscopy (UPS) which is used to determine the structure of the valence band. The He I 21.2 eV photon from a helium lamp is often used in UPS to ionize the valence band electrons off of a surface as shown in Figure 2-16. [18] These electrons are then collected by an electron energy analyzer which allows mapping of the density of occupied electron states in the valence band in the sudden approximation. X-ray photoemission spectroscopy, also shown in Figure 2-16, uses the same principle but uses higher energy x-rays to ionize core electrons. We can then compare this binding energy information to known data to determine the molecular content of a material.

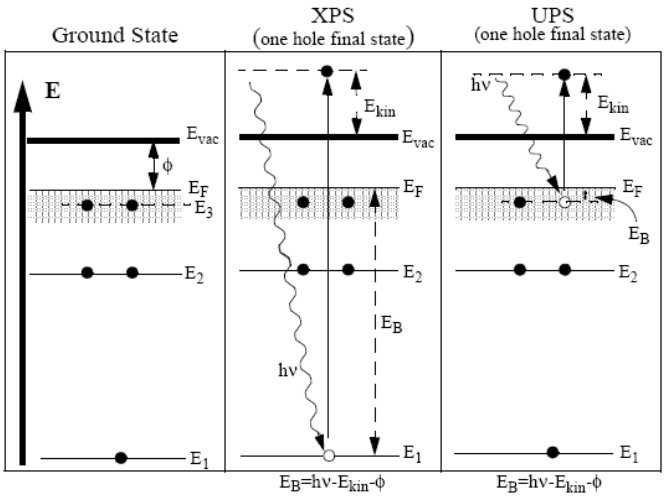

Figure 2-16. Schematic diagram of x-ray and ultraviolet photoemission spectroscopy. [18]

Inverse photoemission spectroscopy (IPES) works on the opposing principle from PES as shown in Figure 2-17. Now, electrons of known energy are aimed at a surface and captured in unoccupied states above the Fermi level. A Geiger-Müller detector is then used to measure the energy of the photon that is released and allow mapping of the conduction band density of states. [18]

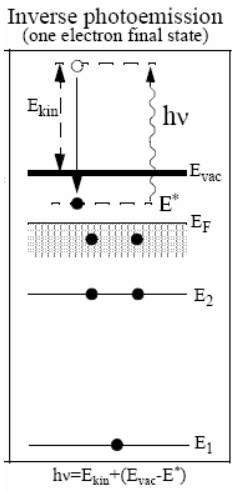

Figure 2-17. Schematic of inverse photoemission spectroscopy (IPES). [18]

2.6. Boron Carbide p-n Junction Diodes.

Boron carbide semiconductors may be grown by plasma enhanced chemical vapor deposition (PECVD) of carborane molecules. These boron carbides have an approximate stoichiometry of "$C_2B_{10}H_x$" (where x represents up to ~5% molar fraction of hydrogen), and form n- or p-type films presumably as a result of differing electronic structures which originate from differences in polytype (molecular structure). [3,19]

2.6.1 Boron Carbide Semiconductor Source Molecules

The two source molecules used in this experiment are orthocarborane (*closo*-1,2-dicarbadodecaborane) and metacarborane (*closo*-1,7-dicarbadodecaborane). Both carborane molecules have the stoichiometric formula $C_2B_{10}H_{12}$ but differ in the placement of one of the carbon atoms (blue) within the icosahedra as shown in Figure 2-18. [3] This seemingly minor difference has a noticeable effect on the placement of the Fermi level within the bandgap.

The experimentally determined (combined photoemission (PES) and inverse photoemission (IPES)) bandgap of metacarborane and orthocarborane is shown in Figure 2-18 with the top of the valence band represented as the highest occupied molecular orbital (HOMO) and the bottom of the conduction band as the lowest unoccupied molecular orbital (LUMO).

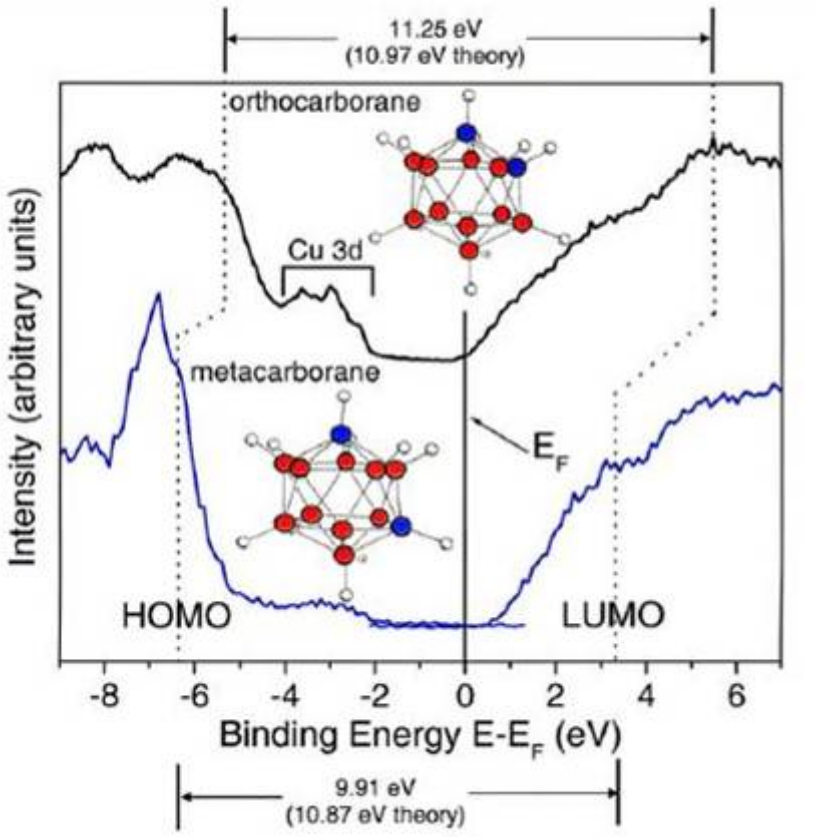

Figure 2-18. The photoemission (negative binding energy) and inverse photoemission experimentally determined bandgap (HOMO–LUMO) of orthocarborane and metacarborane ($C_2B_{10}H_{12}$) where blue atoms are carbon, red are boron, and white hydrogen. Metacarborane was adsorbed on a gold substrate while orthocarborane was adsorbed on copper. The highest occupied molecular orbital (HOMO) represents the top of the valence band and the lowest unoccupied molecular orbital (LUMO) represents the bottom of the conduction band. [3]

When the carborane molecules are exposed to white light in a synchrotron or an electron beam, they dehydrogenate and we see changes in the PES/IPES spectra as shown in Figure 2-19. [3] We see in panels (a) and (b) that as dehydrogenation occurs in metacarborane, the valence band shifts away from the Fermi level indicating n-type properties. Orthocarborane appears p-type as the valence band shifts towards the Fermi level and lower binding energies as seen in panels (c) and (d).

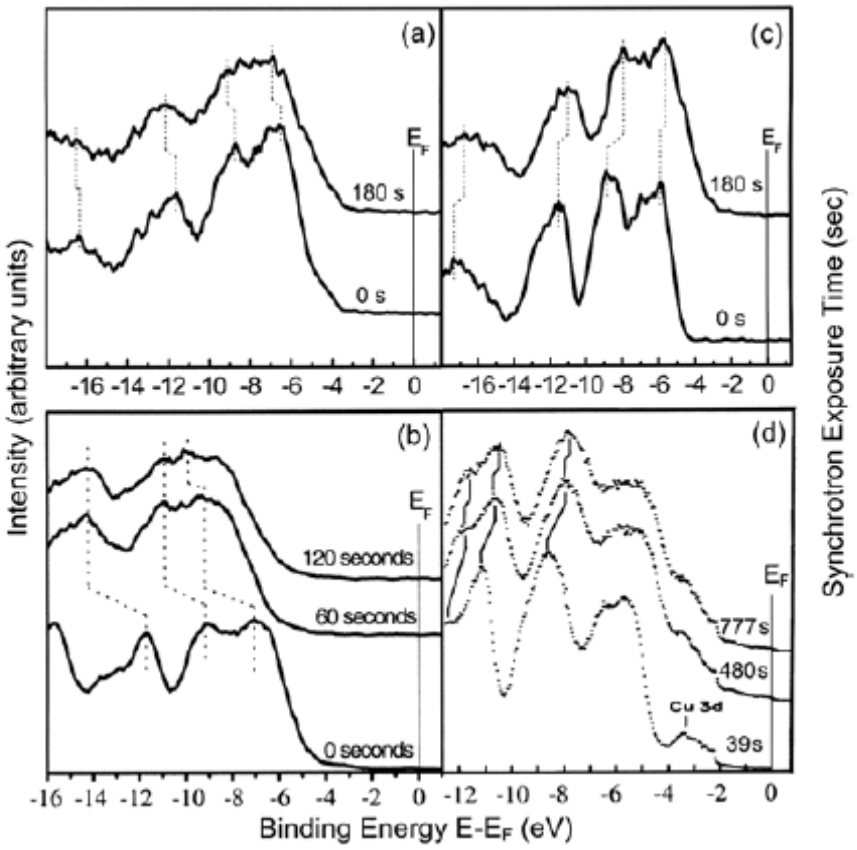

Figure 2-19. Changes in the band structure of metacarborane and orthocarborane after exposure to zero order (white) synchrotron light at temperatures of approximately 105 K. The exposure causes de-hydrogenation of the molecules. The binding energies of the photoemission spectra of metacarborane adsorbed on Ag (a) and Au(111) (b) shift away from the Fermi level indicating n-type behavior. The photoemission observe binding energies of orthocarborane adsorbed on polycrystalline Ag (c) and Cu(111) (d) shift towards the Fermi level indicating p-type behavior. [3]

2.6.2 Boron Carbide Dopants

While the different polytypes of boron carbide form p- and n-type materials, there is still an interest in dopants that allow variations in the carrier concentrations or different mechanical properties of the film. Boron carbide has been successfully doped n-type with iron, vanadium, chromium and nickel. [1,4,[5],10,11] There has been less success in

finding a p-type dopant. From the Seebeck coefficient of films derived from icosahedral boron, there are indications that Co may be a p-type dopant of boron rich films. [5]

There have also been unsuccessful doping attempts, such as mercury, which clustered in the film and did not increase the carrier concentration. [8] If cobalt is indeed a dopant for semiconducting boron carbides, the challenge is then how to introduce cobalt into a growing film in sufficient concentration to increase carriers without clustering of this extrinsic impurity.

For this research, cobaltocene as shown in Figure 2-20 [20], was introduced with an orthocarborane source molecule during plasma enhanced chemical vapor phase deposition (PECVD) similar to the nickel doping technique previously found to be successful. [1,4,10,11] Cobaltocene has previously been shown to successfully dope SnS_2. [21]

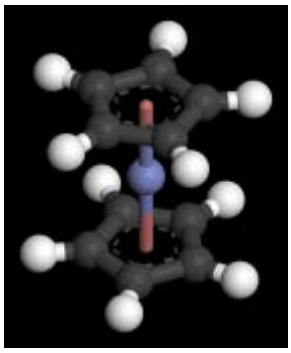

Figure 2-20. Diagram of the cobalt metallocene, cobaltocene. The cobalt atom is bonded to two cyclopentadienyl rings (C_5H_5) and largely dissociates when exposed to an electron beam or plasma enhanced chemical vapor deposition. [20]

Molecular cobaltocene adsorbed on a Cu(111) surface has been previously found to decompose under exposure from zero order synchrotron white light and was expected to successfully decompose using a 500 eV electron gun. Adsorbed molecular cobaltocene

results in photoemission features at binding energies in the region of -5.1±0.2 eV, -9.0±0.2 eV, -12.7±0.2 eV, and -17.3±0.2 eV ($E-E_F$). [21-24] As seen in Figure 2-21, 16L (1 Langmuir = 1.0 x 10^{-6} Torr-second) of cobaltocene adsorbed on Cu(111) at 150 K desorbs from the substrate after irradiation by synchrotron white light leaving the Cu peaks as the most prominent features.

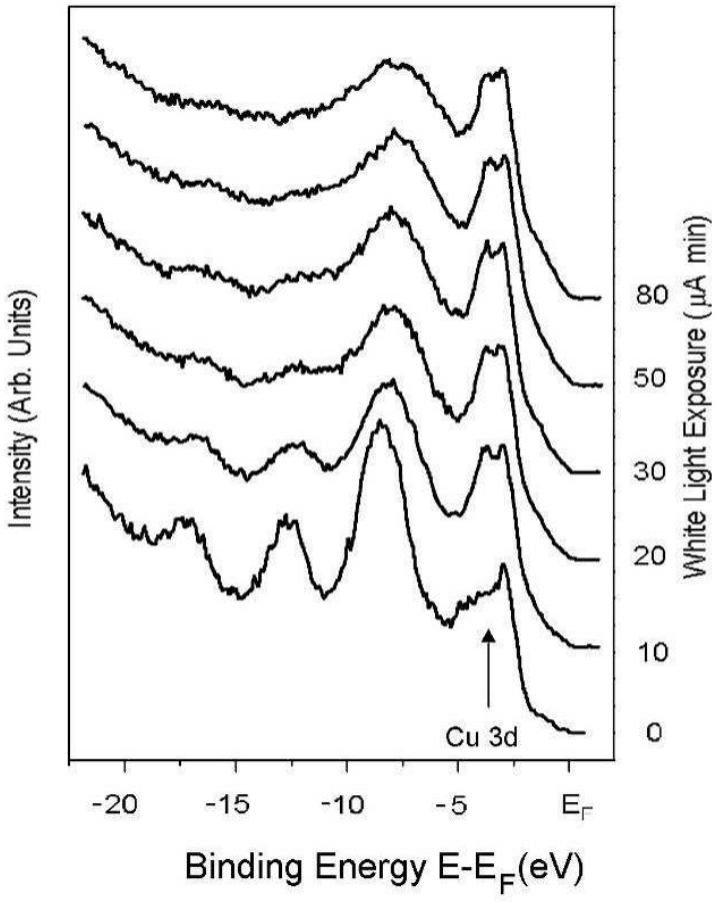

Figure 2-21. Photoemission spectra of 16 L (1L = 1.0 x 10^{-6} Torr.second) cobaltocene adsorbed on Cu(111) at 150 K as a function of white light exposure (exposure = sample current x minutes). The spectra were taken using a 36 eV incident photon energy, with all the photoelectrons collected along the surface normal and a light incidence angle of 40 degrees off the surface normal. [23]

2.6.3 Boron Carbide Heterojunction Diodes

A heterojunction diode is a p-n junction made of two different kinds of material such as p-type boron carbide deposited on n-type silicon as shown in Figure 2-22. [10]

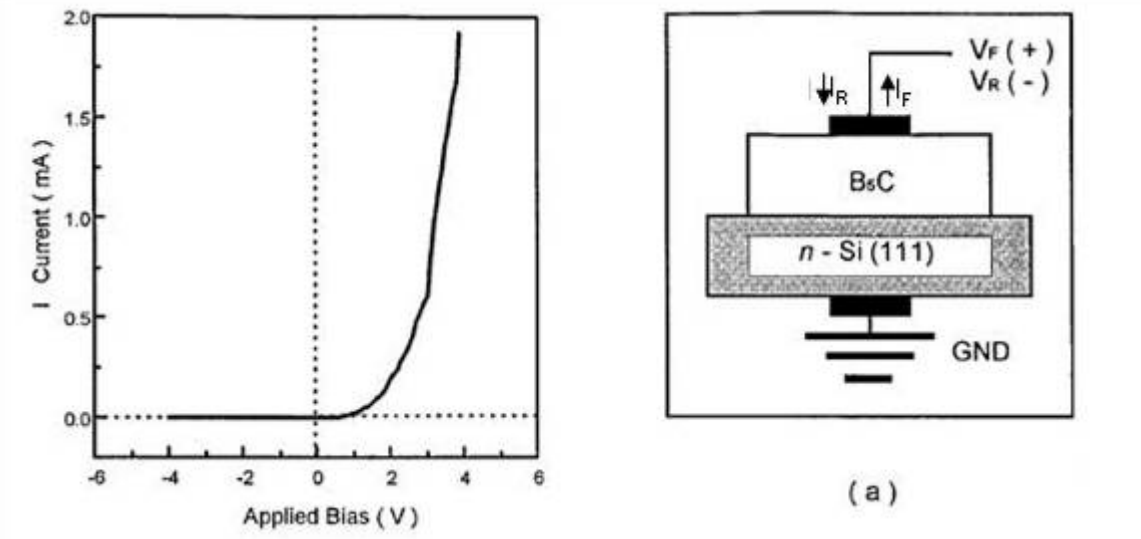

Figure 2-22. I-V curve and schematic of a heterojunction diode grown by depositing a p-type boron carbide film (orthocarborane) on n-type silicon using plasma enhanced chemical vapor deposition. [10]

Nickel doping of boron carbide experiments using a heterojunction determined that nickel is an n-type dopant as shown in Figure 2-23. [1,4,10,11,25] The strong n-type doping of nickel resulted in an n/n+ junction where the n-type silicon was relatively more p-type than the nickel doped orthocarborane resulting in the I-V curve flipping so that forward bias occurred at negative voltages. If cobalt is a p-type dopant, cobalt doping films of decomposed metacarborane on n-type silicon would result in an I-V curve similar to Figure 2-22. Similarly, we could observe n-type doping by doping cobalt into orthocarborane on p-type silicon and observing a reversed I-V curve.

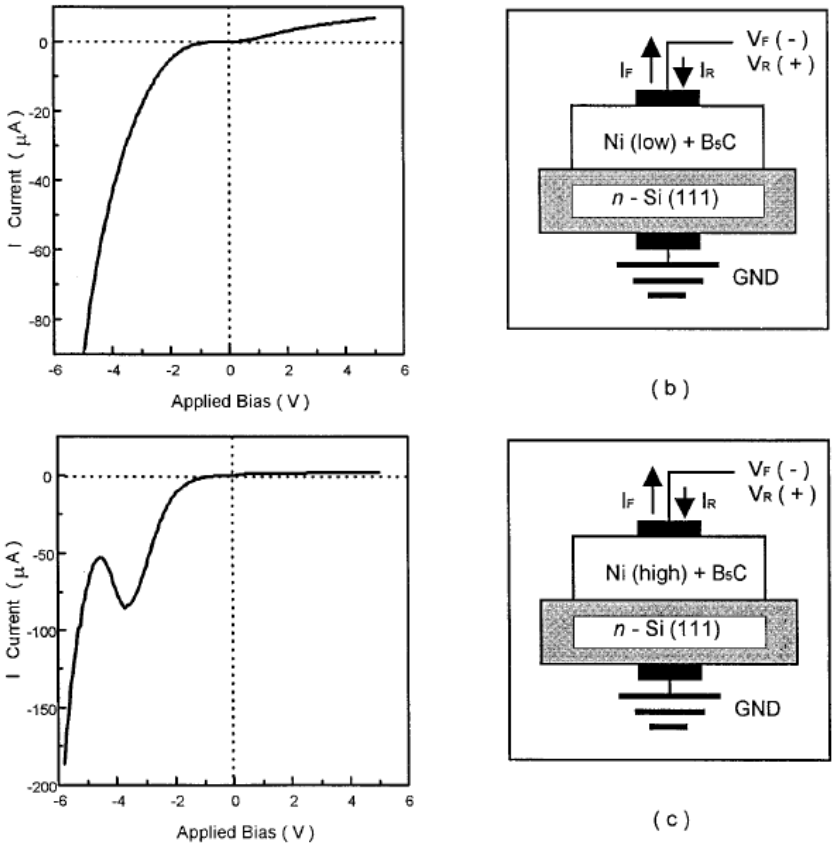

Figure 2-23. Nickel doping of a boron carbide-silicon heterojunction shows that nickel is an n-type dopant as observed by the flip of the I-V curve from Figure 2-22 when a low concentration of nickel was doped in (b). A high concentration of nickel (c) resulted in a tunnel, or Esaki, diode. [10]

2.6.4 Boron Carbide Homojunction/Heteroisomeric Diodes

A further development of boron carbide semiconductors was the fabrication of heteroisomeric diodes where the p-type film is plasma enhanced chemical vapor deposition (PECVD) decomposed orthocarborane and the n-type film is PECVD decomposed metacarborane on a metal substrate as shown in Figure 2-24. [3] Using metal substrates instead of silicon eliminates the possibility of a silicon-silicon dioxide junction forming if the experimental apparatus is unable to sufficiently eliminate oxygen from the system or if we have non-ohmic contacts.

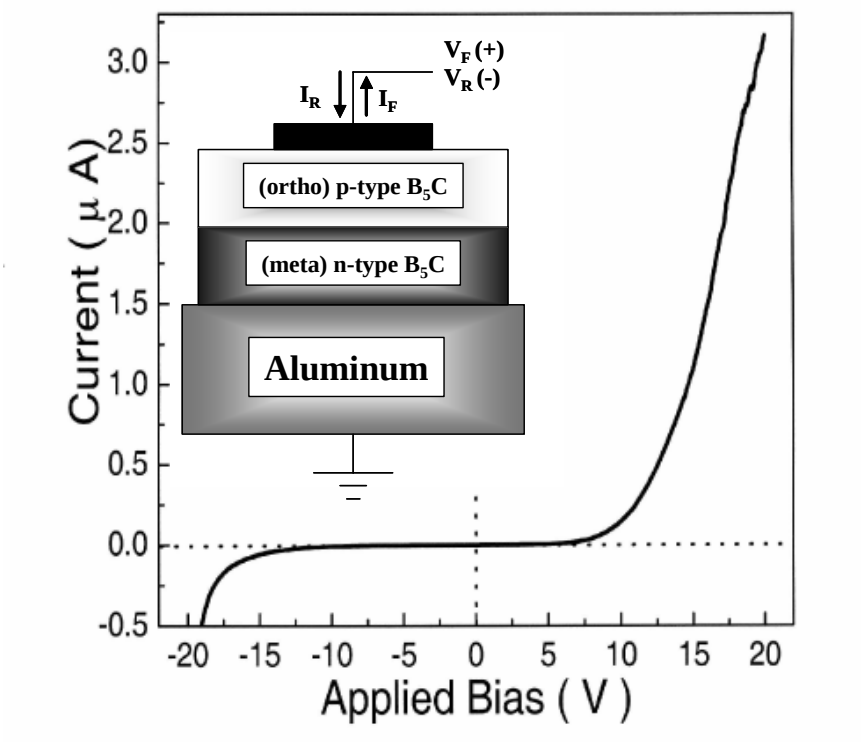

Figure 2-24. The I-V curve of a heteroisomeric boron carbide p-n junction where decomposed orthocarborane forms the p-type layer and decomposed metacarborane forms the n-type layer. Inset is a schematic of the diode. [3]

A boron carbide homojunction diode is fabricated by doping one carborane source layer with extrinsic impurities and then using the same carborane source to form a second layer as shown in Figure 2-25. [1] In Figure 2-25, the normally p-type boron carbide resulting from orthocarborane deposition is doped n-type by nickel and then a p-type layer from continued orthocarborane deposition used to make the p-n junction.

A single layer of doped material would simply be resistive. Adding a second layer of the undoped material then allows the possibility of a junction to form regardless of whether the dopant is n- or p-type if sufficient carrier concentrations are achieved.

In Figure 2-25, if the nickel had been a p-type dopant instead of n-type, the I-V curve would flip and we would be able to determine the p-type doping on that characteristic alone. [1]

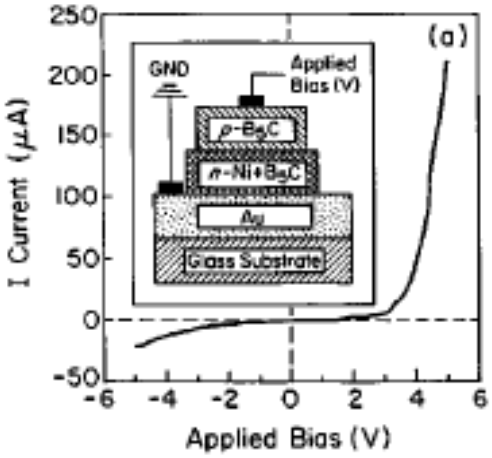

Figure 2-25. The I-V curve of a homojunction boron carbide p-n junction where decomposed orthocarborane forms the p-type layer and is then doped with nickel during decomposition to form the n-type layer. Inset is a schematic of the diode. [1]

3. Experimental Procedures to Determine Electronic Structure of Cobaltocene Doped Boron Carbide Films.

3.1. Apparatus.

Three separate experiments were used to determine how well cobalt doped into a boron carbide film and the band structure changes resulting from cobalt doping. These are ultraviolet photoemission spectroscopy (UPS), inverse photoemission spectroscopy (IPES), and x-ray photoemission spectroscopy (XPS). All three experiments were conducted in a ultra high vacuum (UHV) chamber (Figure 3-1) used by the Dowben group at the University of Nebraska at Lincoln which has a base pressure of 5×10^{-11} Torr. All experiments were conducted using a ~1cm square Si(111) commercially purchased substrate covered with a 1000 Å Au(111) thin film.

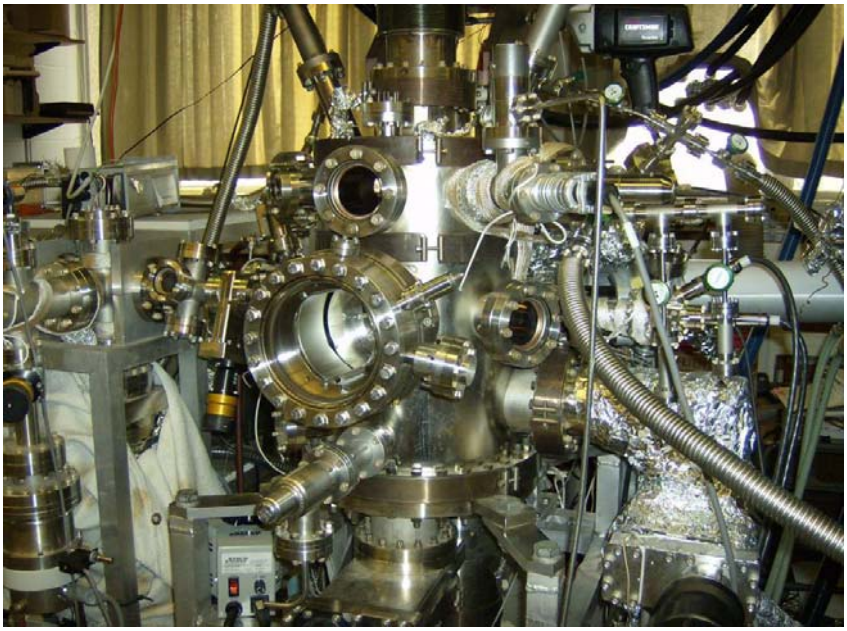

Figure 3-1. Ultra high vacuum (UHV) chamber used to conduct UPS, IPES, and XPS experiments on cobalt doped boron carbide films.

3.1.1 Ultraviolet Photoemission Spectroscopy (UPS).

The photoemission spectra were taken using the 21.2 eV He I line from an ultraviolet lamp with the photons directed at the substrate 45° off the surface normal. The photoelectrons are then collected off the surface normal using a hemispherical electron energy analyzer as schematically shown in Figure 3-2. A representative schematic of the required electronics is shown in Figure 3-3 except the electron gun is replaced with the helium lamp and the Geiger-Müller detector is replaced by an electron energy analyzer. [26]

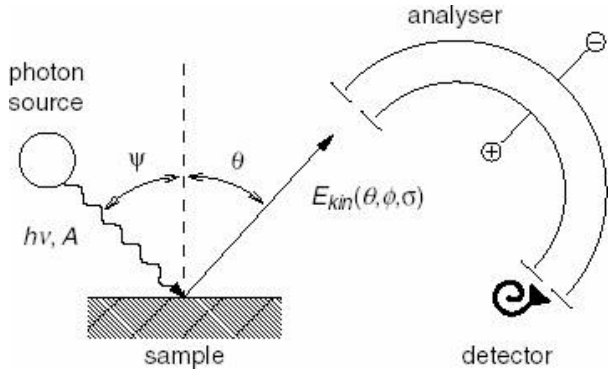

Figure 3-2. Schematic diagram of ultraviolet photoemission spectroscopy equipment with the He I photon source (21.2 eV) at 45° off the surface normal and the energy analyzer along the surface normal. [26]

3.1.2 Inverse Photoemission Spectroscopy (IPES).

For the inverse photoemission studies (IPES), a Geiger-Müller detector fitted with a SrF_2 window of 9.5 eV pass energy was used in conjunction with an Erdman-Zipf electron gun. [27] The overall energy resolution was experimentally determined previously to be about 0.40 eV. All IPES spectra were collected with the electron gun at

normal incidence and the detector positioned at 45^{o} off the surface normal. A general schematic of the electronics is shown in Figure 3-3. [28]

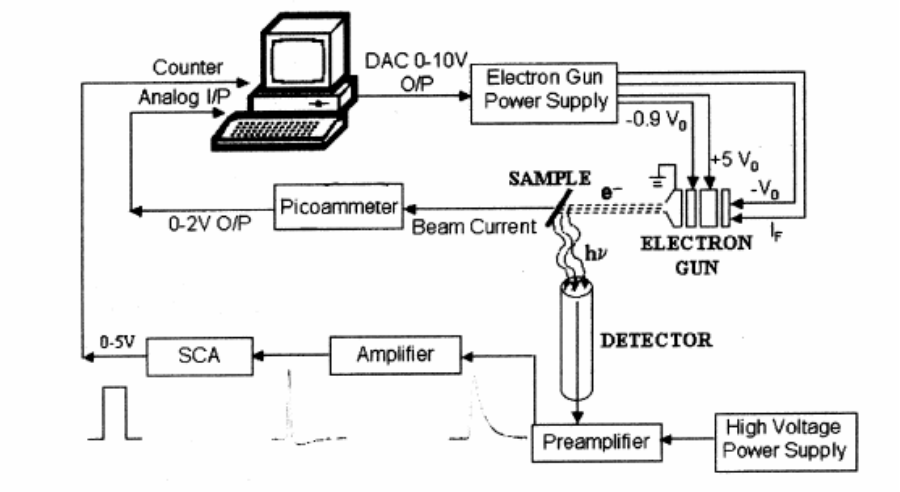

Figure 3-3. Schematic of the components required for inverse photoemission spectroscopy (IPES). [28]

3.1.3 X-ray Photoemission Spectroscopy (XPS)

The apparatus required for the x-ray photoemission spectroscopy studies is nearly identical to that for ultraviolet photoemission spectroscopy. The same electronics and detector are used but the photon source is now an x-ray gun utilizing a magnesium K_{α} 1254 eV line. The x-ray source is 45^{o} off the surface normal and the photoelectrons were again collected along the surface normal.

3.2. Experimental Procedures.

3.2.1 Substrate Preparation.

After cleaving the Si/Au(111) sample substrate to the appropriate dimensions and attaching to conducting tantalum foil wires, the sample was placed in a load lock, which was pumped down overnight. The sample was then maneuvered into the substrate holder

in the UHV chamber. The substrate holder is connected to a cold finger via tungsten wires. The cold finger is cooled by a liquid nitrogen reservoir and the temperature measured via a type-K thermocouple. It takes ~ 2 hours to cool the sample down to 180-200 K where adsorption and characterization take place.

Once the temperature stabilized, the metal surfaces of the substrate and holder are cleaned by argon ion sputtering. Prior to deposition of any precursors, an ultraviolet photoemission spectra was taken to verify the Au(111) is clean by comparison to standard gold spectra and to establish the position of the Fermi level. The binding energies are referenced to the Fermi level of Au and calibrated by the tantalum foil. [3] Once the Au(111) is clean, deposition begins.

Three separate series of depositions were conducted in order to ensure results could be duplicated.

3.2.2 Deposition and Spectroscopy.

The first deposition series on 8 Dec 06, consisted of admitting 50 Langmuirs ($1L=10^{-6}$ Torr-second) of metacarborane into the UHV chamber through a standard leak valve at a pressure of 2×10^{-6} Torr for 25 seconds. UPS was then run to observe the increasing metacarborane and decreasing gold peaks in the spectra. The UPS spectra collection was ran for 50 iterations in order to get good statistics and reduce noise. This process of adding 50L of metacarborane followed by UPS was repeated three times followed by three more iterations with 25L until the gold peaks and the Fermi edge had nearly disappeared. The metacarborane was then decomposed by manually slewing the electron gun over the sample using 500 eV electrons with a current density of 1 A/m^2 for

five minutes. UPS showed that decomposition was not complete so 25L of metacarborane was added and decomposition repeated for three minutes. UPS was then repeated and verified that the decomposed metacarborane spectra matched previous results. [29]

60L of metacarborane was then admitted to the chamber followed by a series of 10-20L adsorptions of cobaltocene followed by UPS. After seeing no change in the UPS spectra, the cobaltocene was increased to 200L for two iterations and then four iterations of 400L until a change was noticed in the spectra. The cobaltocene sample vial required heating with a heat gun in order to sublimate sufficient material to increase the pressure. The final cobaltocene depositions occurred while simultaneously decomposing with the electron gun. The final UPS spectra did not show clear peaks so x-ray photoemission spectroscopy (XPS) was run to verify cobalt in the film.

After pumping the chamber down for three days to remove contaminants, the second series of depositions was conducted on 12-13 Dec 06. The substrates were prepared, cooled, and characterized as previously discussed. In addition, a baseline inverse photoemission spectra was taken of the Au(111) sample. 350L of metacarborane was admitted to the chamber using the technique previously mentioned and baseline UPS and IPES spectra ran. Decomposition used the same parameters as 8 Dec 06 but the times were increased significantly.

The initial metacarborane adsorption was decomposed for 15 minutes with the electron gun and then continued to decompose for another 15 minutes while 112L of metacarborane was admitted to the chamber. Baseline UPS and IPES spectra for the decomposed metacarborane were then taken. A one hour session of alternating admitting

100L of metacarborane and 100L of cobaltocene while decomposing with the electron gun resulted in ~3000L of each source compound decomposed on the Au(111) sample. Final UPS, IPES, and XPS spectra were taken at low temperature (~200 K). After warming the samples to room temperature (~296 K) overnight, UPS, IPES, and XPS were taken of the doped boron carbide films which completed this portion of the experiment.

4. Diode Growth and Characterization Experimental Procedures.

4.1. Apparatus.

The fabrication and characterization of diodes consisted of three primary steps: deposition of the boron carbide film in a plasma enhanced chemical vapor deposition (PECVD) reactor; fabrication of the electrical contacts; and measurement of the current-voltage (I-V) characteristics.

4.1.1 Plasma Enhanced Chemical Vapor Deposition.

The plasma enhanced chemical vapor deposition (PECVD) system consists of 4 major assemblies as shown from left to right in Figure 4-1 and Figure 4-2: the electronics package; gas flow and precursor assembly; reactor chamber; and vacuum system.

The electronics package consists of radiofrequency (RF) plasma generation, temperature control, vacuum monitoring, and turbo pump control. RF plasma is generated inside the reactor by a 13.56MHz RF Plasma Products Inc. Model MN 500 RF signal generator with a 50Ω matching unit. The RF power generated is not currently instrumented but a series of LEDs shows the relative power output. Typical power applied is one LED "bar" showing which is estimated to be ~50W.

There are four temperature controllers in the electronics package. One for the argon supply line, two shared by the three precursor lines, and one for the substrate heater in the reactor. The substrate temperature controller is a Brand-Gaus Model 611 Profiling Temperature Controller which allows programming of cool-down or heat-up profiles. The other three temperature controllers are Brand-Gaus Model 411's which do not have programmable profiles. Type K thermocouples are used for each controller.

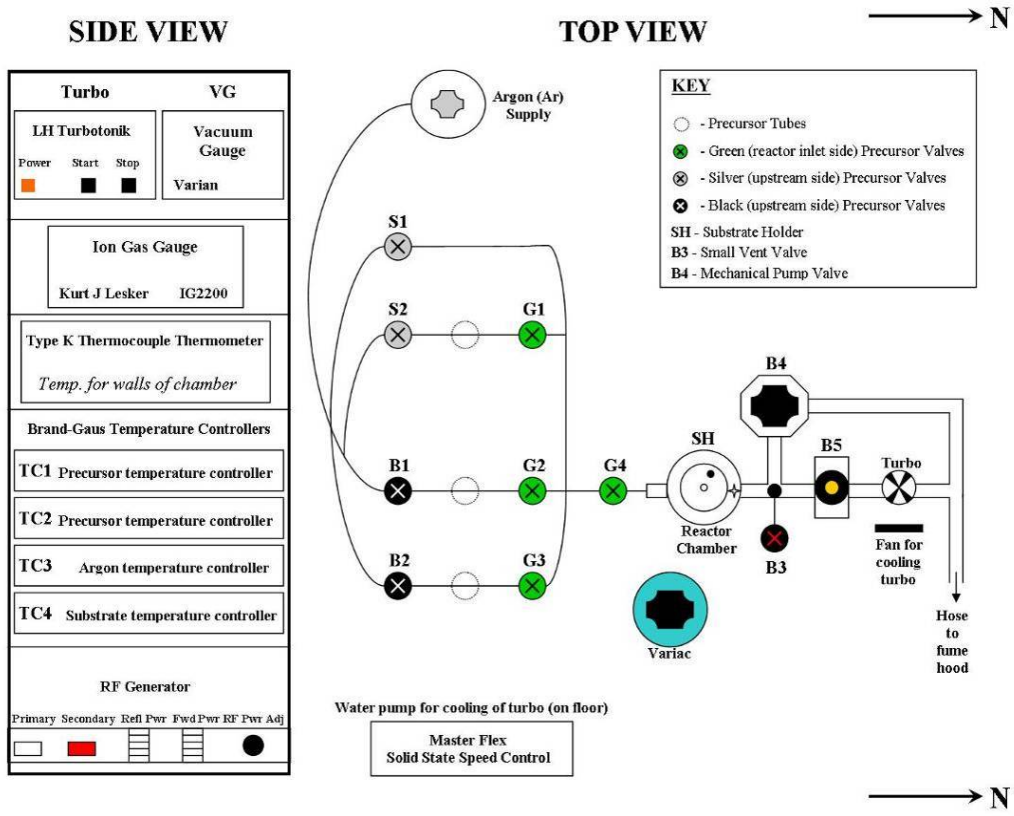

Figure 4-1. Schematic of the four major assemblies of the PECVD reactor system. From left to right: electronics package; gas flow and precursor assembly; reactor chamber; and vacuum system.

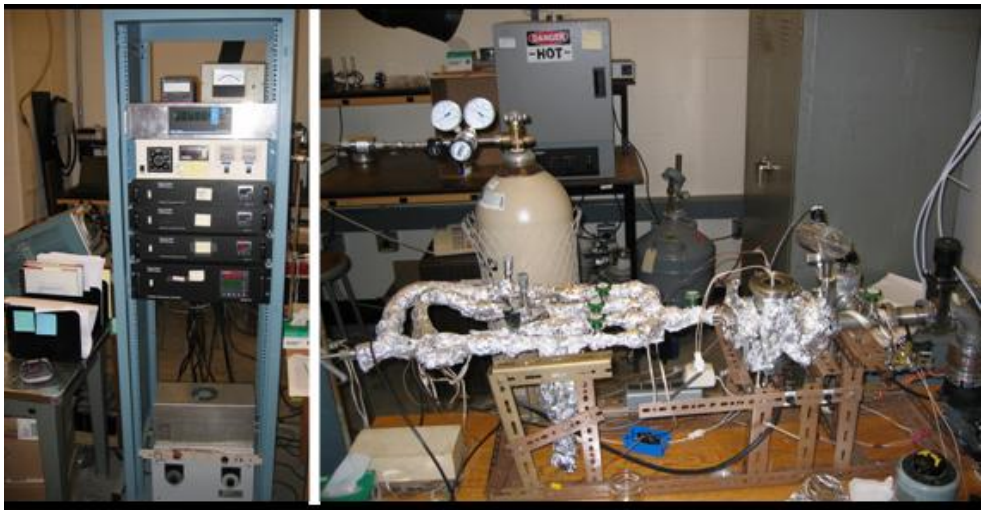

Figure 4-2. Split view picture of PECVD reactor assembly.

Vacuum monitoring consists of a Varian 802-A thermocouple vacuum gauge using a Lesker 4 pin thermocouple placed on the back side of the reactor. A Leybold Vacuum Inc., Turbotronik NT 50 turbo pump controller controls the turbo pump.

The gas flow and precursor assembly controls the argon and precursor flow into the reactor as shown in Figure 4-1. 99.9% ultra high purity argon from Linweld, Inc. is used as a carrier gas and is regulated to ~20 psi. A 0.003-micron Aeronex Model SS-35-KF-I-4R inert gas purifier further purifies the argon. The three precursors are stored in glass vials with stainless steel conflat flanges as shown in Figure 4-3

Figure 4-3. Precursor glass vial with stainless steel conflat flanges and Swagelok fittings. Not shown is the thermocouple, heating tape, or insulating aluminum foil.

The three vials are filled with orthocarborane, metacarborane, and cobaltocene which sublime well near room temperature. Each vial has a taped-on type-K thermocouple, is wrapped in heating tape, and covered in aluminum foil in order to maintain temperature control using the Brand-Gaus 411 temperature controllers. Swagelok stop valves are located on the reactor side of each vial. Swagelok and Whitey needle metering valves are located on the argon side in order to control the partial pressure of the precursor into the reactor. Precursor flow into the reactor is controlled by a combination of precursor temperature and argon carrier gas flow rate. All connecting tubing is stainless steel and wrapped with the same heating tape as the corresponding

precursor vial as well as aluminum foil to keep precursor gases sublimed until they reach the reactor.

The reactor consists of a 3” four-way stainless steel cross with quick flanges using Viton o-rings as schematically shown in Figure 4-4 and Figure 4-5.

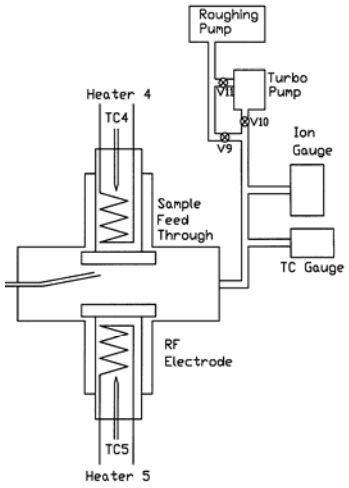

Figure 4-4. Schematic view of the plasma enhanced chemical vapor deposition reactor chamber.

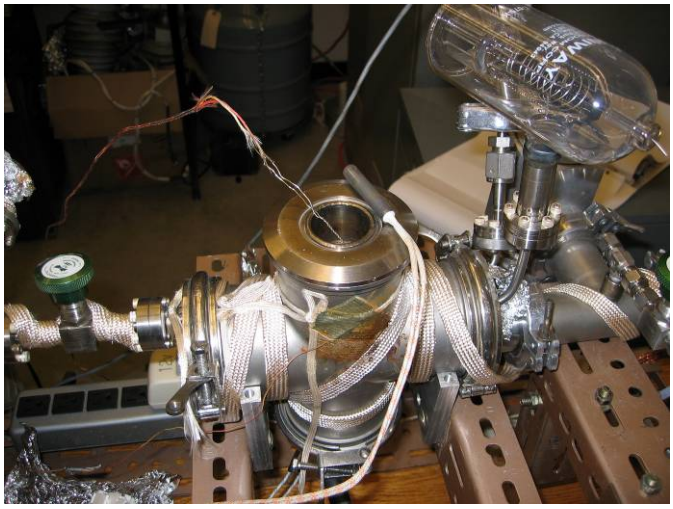

Figure 4-5. Reactor chamber made of a 4-way 3” cross using quick flanges. Precursors enter from left and vacuum pumps connect from the right. The RF plasma electrode is installed in the bottom flange. The top flange is removed to install substrates. Shown on the substrate holder is the substrate cartridge heater and thermocouple wire. Thermocouple vacuum gauge is shown behind glass ion gauge.

The precursor side of the cross (at left in Figure 4-4/Figure 4-5) uses a flange with a glass view port, to visually verify a plasma, and the precursor inlet tube. The vacuum pump side of the cross (at right of Figure 4-4/Figure 4-5) uses a quick flange which has three connections for the thermocouple vacuum gauge, ion gauge (not used), and vacuum pumps. The flange at the top of the cross is the substrate holder and is easily removable. The substrate holder is a 2.75" wide flat aluminum disc 0.25 inch thick at the end of a steel rod as shown in Figure 4-6.

Figure 4-6. Substrate holder (top reactor flange). Shown is an aluminum mask that holds the metal or silicon substrates in place.

The substrate holder is drilled down the center to allow the use of a 400W cartridge heater and type-K thermocouple controlled by the Brand-Gaus Model 611 Temperature Controller. The bottom flange is similar to the top flange as it has a steel tube with an aluminum disk at the end. The flange is connected to the RF plasma generator and the aluminum disk acts as the electrode. The heating tapes shown on the reactor are used to bake out the reactor between growing sessions.

The vacuum system utilizes a turbo pump in parallel with a mechanical roughing pump. The Edwards Model E2M2 roughing pump reduces the system pressure to ~1 mTorr. The Leybold Turbovac 50 turbo pump is capable of pumping to ~1 μTorr.

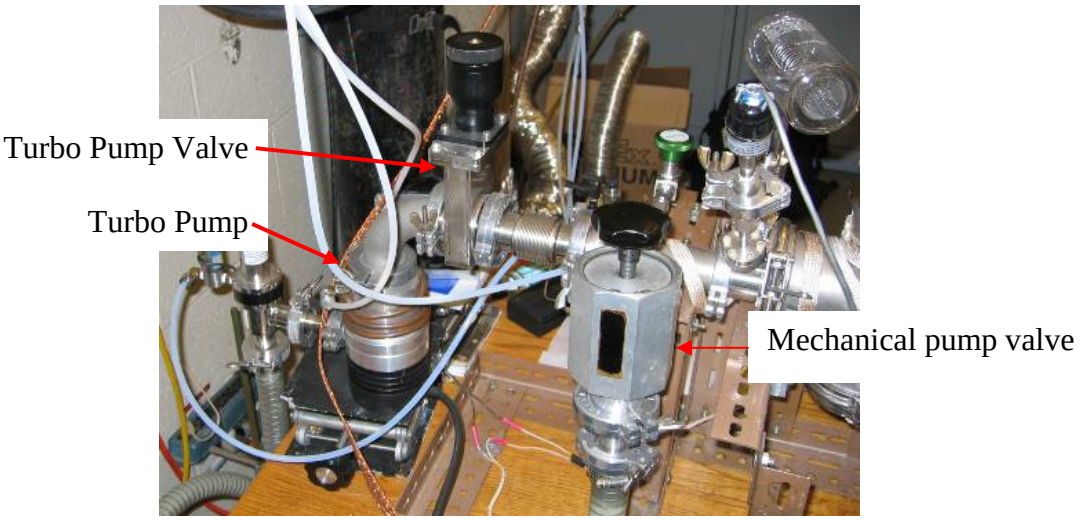

Figure 4-7. Vacuum pumping system. Separate valves can isolate the reactor from the mechanical pump (on floor) or turbo pump (at left on stand).

Both pumps are connected to the reactor as shown in Figure 4-7 but are isolated from each other by manual gate valves. The turbo pump exhausts into the mechanical pump inlet while the mechanical pump exhausts into a fume hood. An accessory fan is used to cool the turbo pump. A molecular sieve trap at the inlet to the mechanical pump protects the pump oil from impurities and keeps pump oil out of the reactor and turbo pump. Regular pump ballasting and reactor bake outs are necessary to keep pressures low.

4.1.2 Contact Sputtering.

The contact sputtering machine is a Technics Hummer III used with a gold target. Copper was originally used but found to oxidize too quickly. The system uses ultra pure

argon from Linweld, Inc. as a carrier gas and a mechanical roughing pump to achieve the normal starting vacuum of <10 mTorr.

4.1.3 Resistivity/I-V Curve Testing

The resistivity and current-voltage (I-V) measurements of the films was conducted using a Keithley 6517A Electrometer. The electrometer is connected to a laptop computer via a IEEE-488 General Purpose Interface Bus (GPIB) cable and card. The electrometer is controlled by Labview software which has options for starting and ending voltage, voltage step size, voltage hold time, and a two way switch.

All testing of diodes is done in the dark under a box which is covered in aluminum foil connected to a common ground as shown in Figure 4-8.

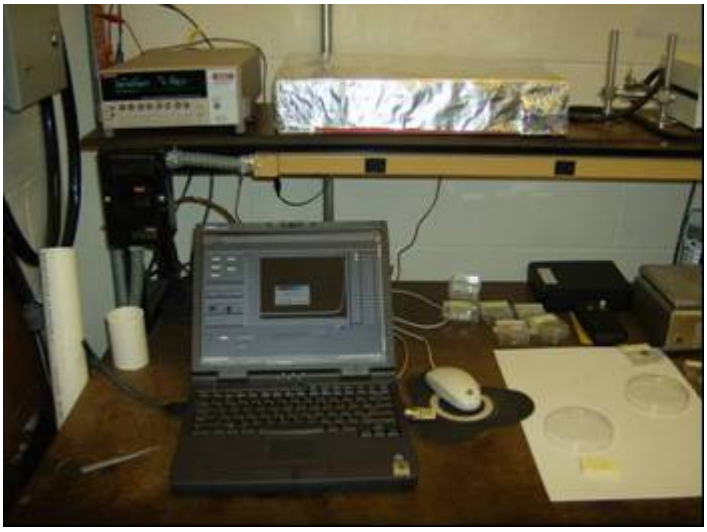

Figure 4-8. I-V curve measurement system consisting of a laptop running Labview software which controls a Keithley 6517A Electrometer over a IEEE-488 interface. The aluminum covered box ensures the sample is tested in the dark to avoid photoconduction.

4.2. Experimental Procedures.

4.2.1 Heterojunction Diode Growth Procedures.

In order to grow a heterojunction film (boron carbide on a silicon substrate), two each p- and n-type silicon substrates were prepared following the detailed procedures in appendix B. The wafers are sourced from Wafernet, Inc. and have resistivities of 10-20 Ω-cm (p-type) and 5-10 Ω-cm (n-type). Example films grown on silicon substrates are shown in Figure 4-9 prior to contact fabrication.

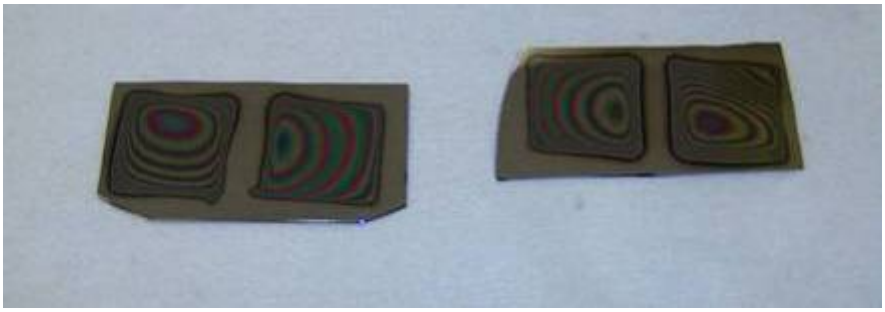

Figure 4-9. Heterojunction boron carbide films on silicon substrates. The rings can be used to roughly determine the film thickness and result from the flow characteristics of the nozzle and reactor.

After cutting the silicon substrates to approximately 2" x 1", the type of silicon is etched on the back of the substrate to avoid mistaking the silicon type. The substrates are then cleaned in acetone and ethanol ultrasonic baths for 10 minutes each to remove organic contaminants. The silicon dioxide (SiO_2) outer layer is then removed by etching the substrates in hydrofluoric acid (HF) for at least ten minutes. The substrates are then placed in deionized, distilled water that has been deoxygenated by nitrogen bubbling to keep the native silicon oxide from reforming.

The cleaned substrate is then mounted to the substrate holder using an aluminum mask with four 1.5cm squares and placed in the reactor for deposition as described in detail in appendix A. The reactor is pumped down to approximately 10^{-3} Torr with the mechanical roughing pump followed by pumping with the turbo pump. The substrates are heated to 345°C and then pumped with the turbo pump down to approximately 10^{-6} Torr for ten minutes. 200 mTorr of 60°C argon is then bled into the system and the substrates plasma etched at ~50W for 20 minutes. During etching, the carborane precursors and cobaltocene are heated for at least ten minutes to ensure uniform temperature and sublimation occurs.

After argon etching, the plasma is stopped and the argon pressure reduced to 150mTorr. The desired partial pressure, typically 25-50 mTorr, of the carborane precursor is then added to the system. Once stabilized, the desired partial pressure of the cobaltocene, typically 25-100 mTorr, is added into the system and the ~50W plasma started again. The doped film is then deposited for the desired period of time, typically 10-45 minutes.

After the desired deposition time, the precursor and argon valves are closed and the reactor pumped back down to about 10^{-3} Torr. The precursor and argon heaters are turned off and the substrate heater programmed to slowly cool down over about a three hour period to avoid film cracking due to the different temperature coefficients of boron carbide and silicon. Electrical contacts are then fabricated as described below in 4.2.3.

4.2.2 Homojunction Diodes Growth Procedures.

In order to grow a homojunction diode, four metal substrates are prepared following the detailed procedures in appendix B. The substrates used were 99.99+% .125mm thick silver, aluminum, and nickel sheets from Sigma-Aldrich, Inc.

The substrate preparation procedures are similar to those discussed in 4.2.1 for silicon substrates except there is no requirement to etch in HF or to use deionized water.

The deposition procedures are also the same as for the heterojunction in 4.2.1 with the exception of one additional process. After the doped layer is deposited on the metal substrate, the precursor and cobaltocene valves are closed and the plasma turned off. The system is then "flushed" with ~2000 mTorr of argon for a minute to remove the cobaltocene vapor from the reactor.

The argon pressure is then returned to 150 mTorr and the desired partial pressure of the same carborane source used in the first layer is added to the argon carrier gas. Once the desired pressure is reached, the plasma is restarted and the undoped boron carbide film deposited for the desired period of time. The system is then shut down as described 4.2.1 as well as in detail in Appendix A.

4.2.3 Electrical Contact Fabrication

Ohmic contacts are fabricated on the boron carbide and substrate surfaces in order to provide a means to measure the resistivity and current-voltage (I-V) characteristics of the potential diodes. A detailed description is in Appendix C.

After removing three of the cooled films from the reactor, they are placed in a 1" square aluminum mask with nine 1 mm holes drilled in the top plate. The fourth film is

returned to the reactor to minimize oxygen exposure as the sputtering machine can only hold three films at once as shown in Figure 4-10. The films are then placed in the sputtering machine which is then pumped down to <10 mTorr. During pump down, venting argon into the dome 2-3 times allows the pressure to ultimately drop lower, probably as a result of desorbing water vapor from the inside of the dome.

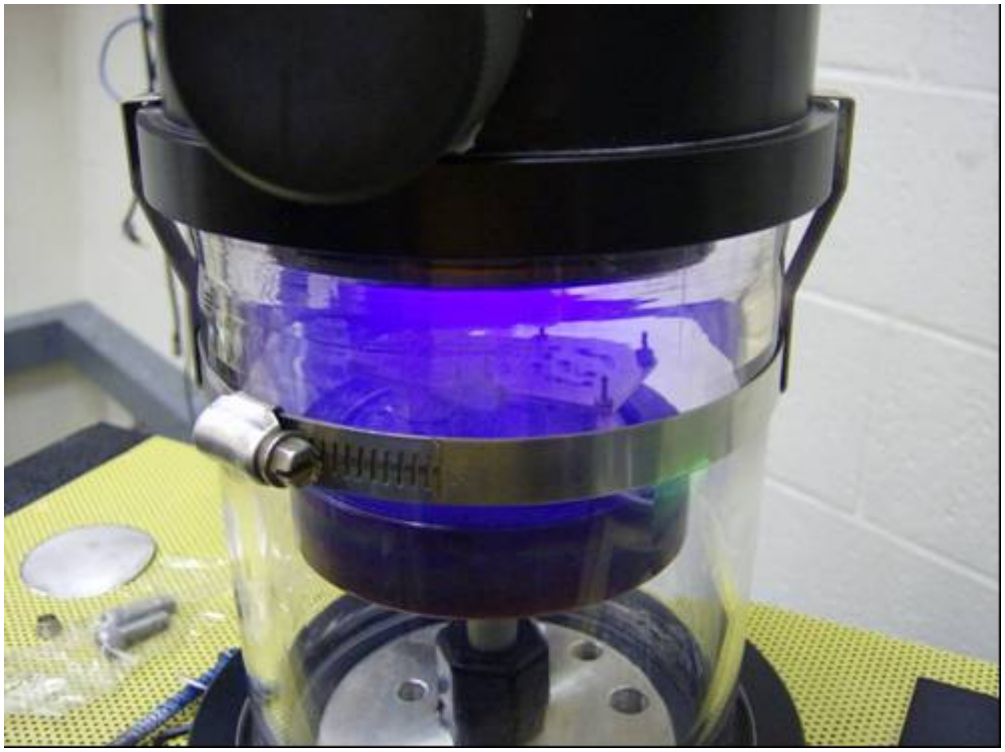

Figure 4-10. Vacuum dome of the Technics Hummer III sputtering machine. A maximum of three 1.5cm films can be sputtered at once. Note the mask with nine 1mm holes. Gold atoms are ionized from the target (top of dome) by the plasma and attracted to the masked films by applying a negative voltage to the electrode the films are sitting on.

After pumping down to <10 mTorr, about 30 mTorr of argon is bled into the system with the metering valve to provide a carrier gas for the plasma. The plasma is struck and the electrode voltage and argon pressure varied until a potential of 9 volts and a current of 10 mA is achieved. Gold is then sputtered for 10 minutes to form an ohmic

contact. Once complete, the films are removed from the vacuum chamber and the process repeated for the fourth film.

After sputtering on the gold contacts, a drop of Epotek P1011S silver epoxy is placed in the center of each sputtered contact as described in Appendix C. A bare, 36 gauge clean copper wire is then inserted in the silver paste. For metal substrates, silver epoxy paste and a copper wire are placed directly on the metal substrate. For silicon substrates, a deburring bit on a rotary tool is used to remove the oxide layer and then silver epoxy is quickly placed on the deburred spot to form the ground contact. The contacts are then heated for 30 minutes at 80°C, followed by an hour at 150°C in order to cure the epoxy. The films are then allowed to cool slowly (about 1 hr) before I-V curve testing. Representative samples of completed contacts are shown in Figure 4-11. During the heterojunction growths on silicon, the contacts were fabricated using only silver epoxy and no sputtering.

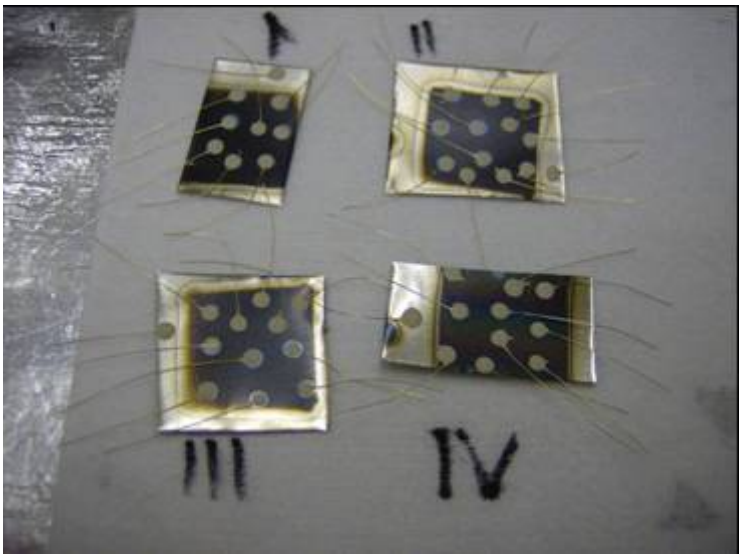

Figure 4-11. Cobalt doped homojunction films showing metal substrates and completed silver epoxy contacts. These are early samples using sputtered copper which was found

to oxidize too quickly (blue tinge around silver contact) and was replaced with sputtered gold.

4.2.4 Resistivity/I-V Curve Testing

The current-voltage (I-V) characteristics of the film were measured in the dark using the equipment described in 4.1.3. The ground contact (Low side) on the electrometer was always connected to the substrate regardless of junction configuration. The Labview software was typically configured to start running from -1 volt to 1 volt in 0.01 volt steps with a voltage hold time of 250ms. The software displays the resulting I-V curve on the screen which allows instant assessment of general resistivity of the film and the possibility of diode action. The data was then saved to a text file for later graphing. The voltages were then slowly increased in order to avoid damaging the film until an assessment was made whether a successful p-n junction had been fabricated.

Resistivity measurements were made by growing cobaltocene-doped meta-carborane films on aluminum substrates with cobaltocene:metacarborane partial pressure ratios of 1:1, 1.5:1, and 2:1. The 1:1 ratio was chosen as a baseline and then progressively increased until the resistivity had significantly decreased. The cobaltocene was heated to 100°C while the metacarborane was kept at room temperature (~24°C) in order to roughly equalize the static vapor pressures. Contacts were fabricated as described above. I-V measurements were then made of each resistor from -1 volt to +1 volt in 0.005 volt steps. The data was then plotted in Origin and a linear fit of the curve determined. The slope of this curve is 1/R as seen from solving Ohm's Law:

$$\Delta V = \Delta IR \rightarrow \frac{\Delta I}{\Delta V} = \frac{1}{R}$$

The resistivity is then calculated from:

$$\rho = \frac{RA}{l} = \frac{A}{l\frac{1}{R}}$$

where A is the area of the contact (7.85 x 10^{-4} cm^2), l is the thickness of the film at that point (estimated from film color at that point), and 1/R is the linear fit of the slope determined from the Origin graphing software. The results of the measured resistivity for the nine contacts on an aluminum substrate are then averaged and the standard deviation calculated.

5. Results and Analysis.

5.1. X-ray Photoelectron Spectroscopy Analysis of Cobalt Deposition

To fabricate semiconducting "$C_2B_{10}H_x$" boron carbide films, metacarborane and metacarborane together with cobaltocene was decomposed on Au(111) at 180-220 K, using electron beam irradiation from a flood gun. After decomposition, X-ray photoemission spectroscopy (XPS) confirmed that cobalt was incorporated in the "$C_2B_{10}H_x$" boron carbide films after cobaltocene and metacarborane decomposition, as shown in Figure 5-1 for the two films grown on 8 and 12 Dec 06. The cobalt $2p_{3/2}$ binding energy is 780.4$\pm$0.3 eV below E_F while $2p_{1/2}$ is 795.6$\pm$0.3 eV below E_F in films formed from both metacarborane and cobaltocene decomposition. This indicates that the resulting inclusion of cobalt is not metallic, which would indicate clustering, as this would result in binding energies of 778.1$\pm$0.1 eV below E_F and 793.2$\pm$0.2 eV below E_F for the cobalt $2p_{3/2}$ and $2p_{1/2}$ binding energies respectively. [30-32].

The very small XPS intensities and low cobalt concentration relative to metacarborane suggest that in spite of comparable exposures of cobaltocene and metacarborane, much of the cobaltocene desorbs in the decomposition process without depositing the cobalt. This desorption is consistent with the results shown in Figure 2-21 where decomposition of cobaltocene adsorbed on Cu(111) by synchrotron white light resulted in significant desorption as seen by increases in the Cu 3d band intensities. The Co XPS spectra seen in Figure 5-1 is very similar to the results of nickel doping of sintered boron carbide presented by Liu. [25]

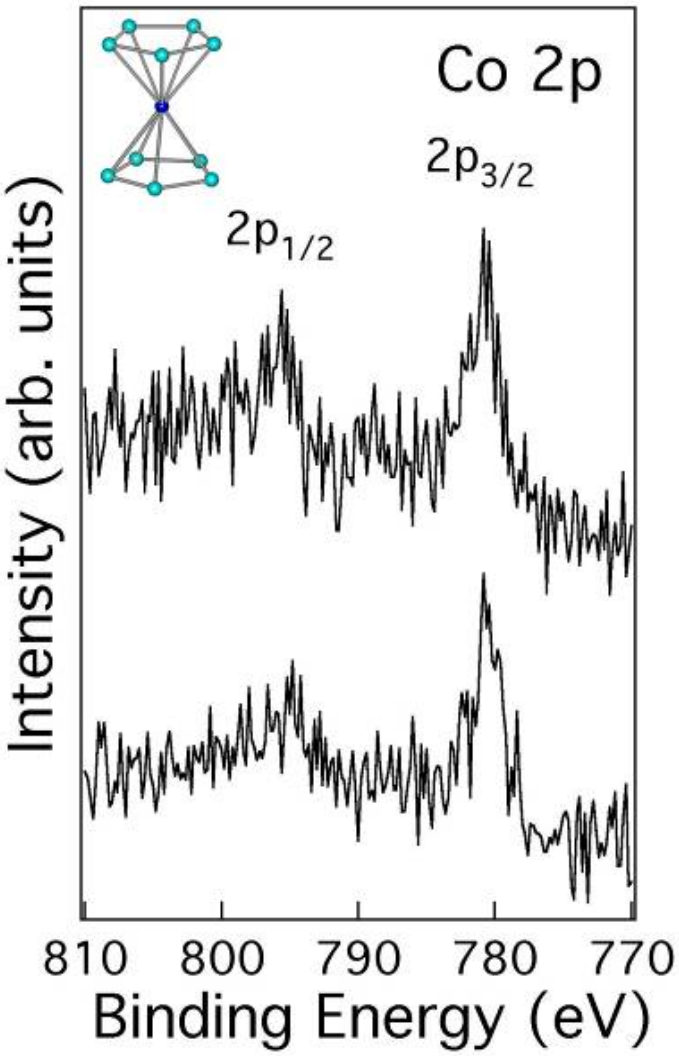

Figure 5-1. X-ray photoemission spectrum (XPS) of Co 2p from 8 Dec 06 (*bottom)* and 12 Dec 06 *(top)* films fabricated by the electron beam decomposition of metacarborane and cobaltocene on Au(111) at 180-220 K. The inset is a diagram of the $Co(C_5H_5)_2$ cobaltocene molecule with the hydrogen omitted.

5.2. Adsorption/Photolysis of Metacarborane/Cobaltocene

Figure 5-2 shows the combined photoemission and inverse photoemission results of a decomposed metacarborane film and a decomposed film of metacarborane and cobaltocene. Figure 5-2 shows that the Fermi level is much closer to the conduction band

edge (the lowest unoccupied molecular orbitals or states) for films formed from metacarborane decomposition alone than is the case for those "$C_2B_{10}H_x$" boron carbide films that include cobalt, from cobaltocene decomposition. This suggests that the cobalt is adding acceptors states (p-type doping) to the "$C_2B_{10}H_x$" boron carbide film formed from the decomposition of metacarborane.

While a comparison of the combined photoemission and inverse photoemission studies suggests that "$C_2B_{10}H_x$" boron carbide films that include cobalt, from cobaltocene decomposition, are more p-type than boron carbide films formed from metacarborane decomposition alone, the majority carriers have not yet been determined directly. Furthermore, photoemission and inverse photoemission are subject to final state and charging effects if the doping concentration is insufficient to dope the semiconductor across the nonmetal to metal transition. [33-34]

Hall Effect measurements to directly determine the carrier type are complicated by the high resistivity of the material and a strong, temperature dependent magnetoresistance.

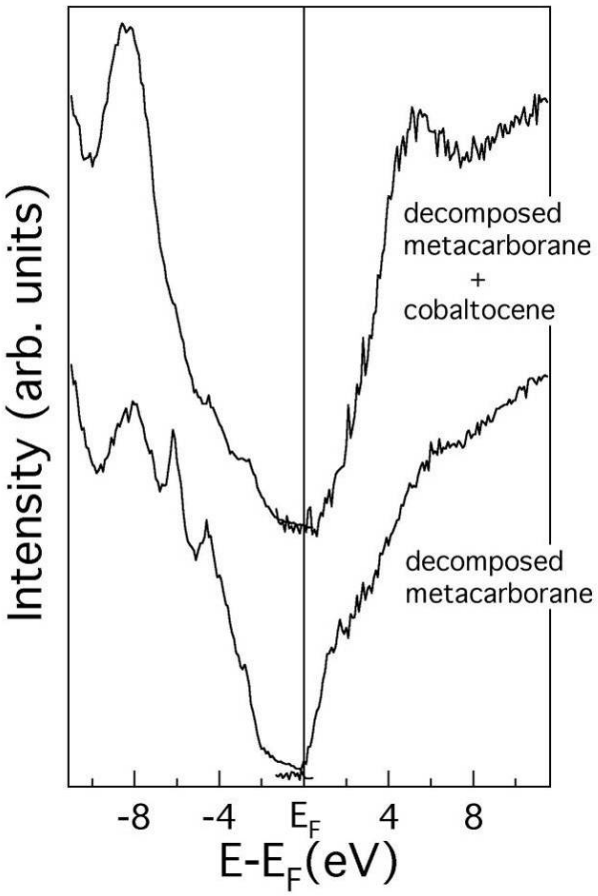

Figure 5-2. Photoemission (UPS) and inverse photoemission (IPES) of "$C_2B_{10}H_x$" boron carbide films formed from the electron beam induced decomposition of metacarborane (*bottom*) are compared with "$C_2B_{10}H_x$" boron carbide films that include cobalt, from electron beam decomposition metacarborane and cobaltocene (*top*). Deposition was undertaken on Au(111) at 180 K. The photon energy is 21.2 eV from a helium lamp.

Figure 5-3 provides strong evidence of final state effects that result in an apparent larger band gap at lower temperatures, indicative of doping levels insufficient for metallization of "$C_2B_{10}H_x$" boron carbide films. At temperatures below 200 K, the band gap inferred from the combined photoemission and inverse photoemission is quite large, while at room temperature, the band gap is closer to the 1.5 eV value of the direct band gap reported for the semiconducting boron carbide polytype formed by PECVD of

metacarborane. [19] At room temperature, this doped film has the conduction band edge placed very close to the Fermi level however, suggesting an n-type semiconductor.

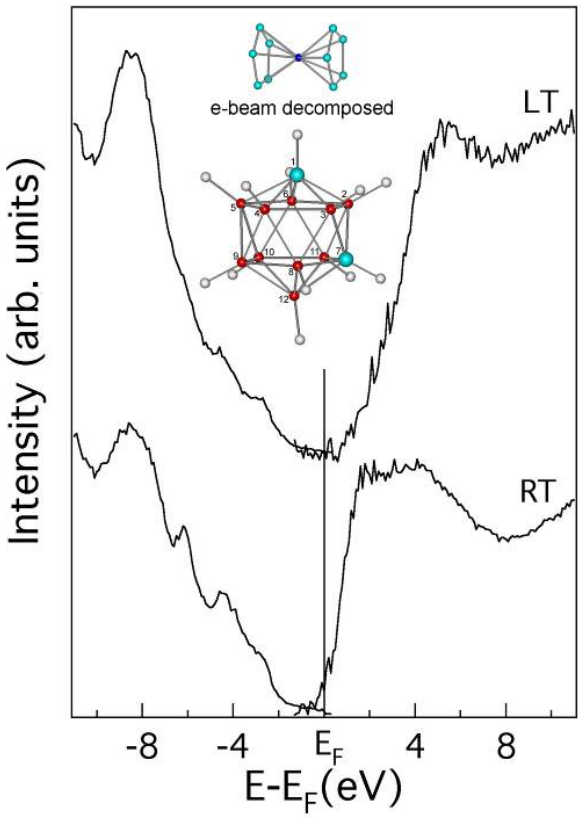

Figure 5-3. Photoemission (UPS) and inverse photoemission (IPES) of electron beam decomposed metacarborane and cobaltocene at 180 K (*top)* and room temperature (*bottom*). The inset shows the metacarborane precursor and cobaltocene without hydrogen.

The shift in the conduction band edge and valence band edge, with temperature, as seen in Figure 5-3, resembles the surface photovoltaic charging seen for a p-type dopant [35,36]; i.e. a shift towards smaller binding energies with decreasing temperatures as photogenerated carriers produce a non-equilibrium emf which offsets some of the original space charge created by the fixed surface charge. The temperature dependent

surface photovoltage effect, observed here, is not, however, compelling evidence to define the majority carrier.

Adsorbed molecular cobaltocene results in photoemission features at binding energies in the region of -5.1±0.2 eV, -9.0±0.2 eV, -12.7±0.2 eV, and -17.3±0.2 eV ($E-E_F$). [21-24] The "$C_2B_{10}H_x$" boron carbide films that include cobalt, from cobaltocene decomposition, show a more significant photoemission feature in the region of -8 eV binding energy as shown in Figure 5-3 and an increase in photoemission intensity in this region is consistent with cobaltocene decomposition as seen in Figure 2-21.

While it is apparent from the shifts in the energy bands that the cobaltocene introduces a dopant, it should be noted again that the majority carrier has not been conclusively established from photoemission, and it is not clear that the cobaltocene introduces an unambiguous p or n type dopant. This is because metacarborane decomposition produces an n-type "$C_2B_{10}H_x$" boron carbide semiconductor, and the cobaltocene material also resembles an n-type "$C_2B_{10}H_x$" boron carbide material based on the position of the Fermi level close to the conduction band edge at room temperature.

5.3. Diode Fabrication.

5.3.1 Heterojunction diodes.

The initial attempt to grow cobalt doped heterojunction films on silicon was not successful although two important lessons were learned.

When cobaltocene was first used as a dopant after growing baseline, undoped films, the films were completely black instead of displaying the fine visible light ring structure previously seen in the undoped films. Because cobaltocene is black and black

films had never been seen before, the assumption was made that there was too much cobaltocene being doped in. This led to a progressive series of films with ever decreasing cobaltocene partial pressures but no sign of the "flip" in the I-V curve that would result from successful doping.

After several films were grown with negative results, an evaluation of how well the contacts were working was conducted by running an I-V curve using the ground contact that was abraded into the silicon and the other contact connected to the silicon dioxide surface. As shown in Figure 5-4, the shape and slope of the I-V curves is indistinguishable indicating that either the contacts or the silicon substrate preparation is not ideal and is likely masking any doping results. In order to eliminate the potential problems caused by using silicon, a shift was made to fabricating homojunction diodes on metal substrates.

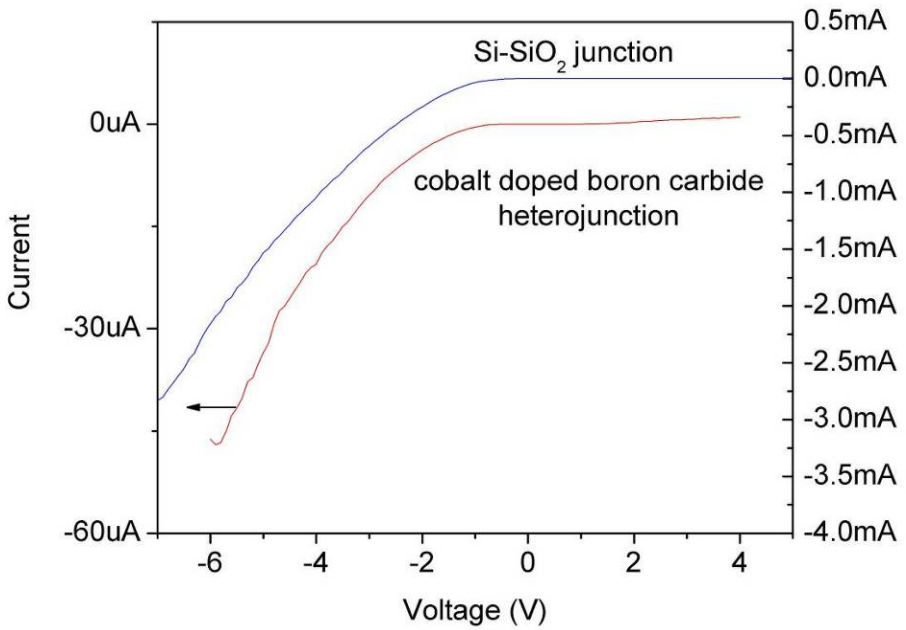

Figure 5-4. Comparison of I-V curves for a cobalt doped boron carbide heterojunction and a silicon-silicon dioxide junction from the same film.

5.3.2 Homojunction diodes.

Coincident with the change to growing homojunctions was a reassessment of how well the cobalt was doping into the boron carbide films. Conducting profilometry on one of the black, cobalt doped, films determined that the film thickness was over 20 microns thick while an undoped film grown for the same period of time was less than one micron thick. The mechanism for this growth enhancement is still unknown. Also, undoped boron carbide films thicker than about one micron tend to "delaminate" or flake off after a few days exposure to air. The much thicker cobalt doped films have not delaminated even after weeks of exposure to air. While not specifically related to doping, this property of cobalt to stabilize the films may have uses that deserve further study.

The question of whether sufficient cobalt was incorporating into the boron carbide film was answered by conducting a resistivity study to determine what growing conditions are required to change the resistivity of the film to something reasonably expected to increase the carrier concentration. Even in PECVD grown films, high partial pressures of cobaltocene do not result in complete metallization of the film, as is clear from the high resistivity values seen in Figure 5-5. Increased partial pressures of cobaltocene, relative to metacarborane, do lead to a decrease in resistivity in the resulting PECVD grown films. The resistivities do not correspond to the room temperature resistivities of graphite (a semimetal with resistivities of $3x10^{-5}$ Ω or less [37]), a likely PECVD decomposition product of large amounts of aromatic hydrocarbon, or an over-doped metallic thin film. Nonetheless, increases in the cobaltocene partial pressures do result in increases in conductivity, indicative of increased carrier concentrations. All the cobaltocene partial pressures studied result in room temperature resistivities that are

lower than the expected 10^{10} to 10^{13} Ohm·cm generally seen for undoped PECVD "$C_2B_{10}H_x$" boron carbides grown from metacarborane. As such, cobaltocene does lead to the doping of "$C_2B_{10}H_x$" boron carbides much like nickel doping, using nickelocene. [1,10]

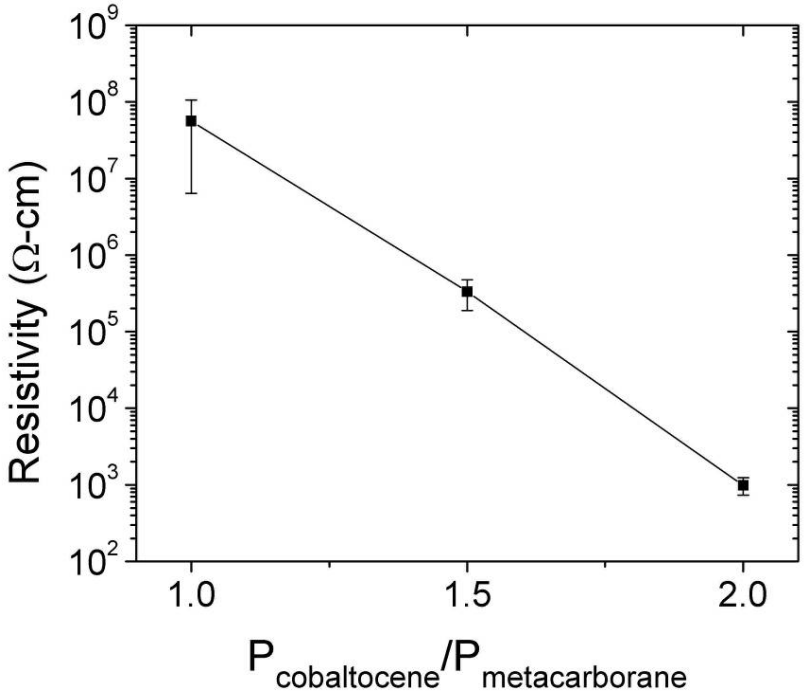

Figure 5-5. Measured resistivities of thin films grown by decomposing cobaltocene and metacarborane on aluminum substrates using plasma enhanced chemical vapor deposition (PECVD). Partial pressure ratios are based on metacarborane sublimed at 296 K and cobaltocene sublimed at 375 K, using 150 mTorr of argon carrier gas at 333 K.

After determining that a partial pressure ratio of 2:1 of cobaltocene to metacarborane was required to reduce the resistivity from ~10^8 Ω·cm to ~10^3 Ω·cm and that the cobaltocene appeared to dope n-type at room temperature from the UPS/IPES studies, a series of homojunction diode films were grown using orthocarborane and

cobaltocene on Al, Ni, and Ag conducting substrates. The growing times were varied in order to optimize the film thickness until a homojunction diode was successfully fabricated as shown in panel b of Figure 5-6.

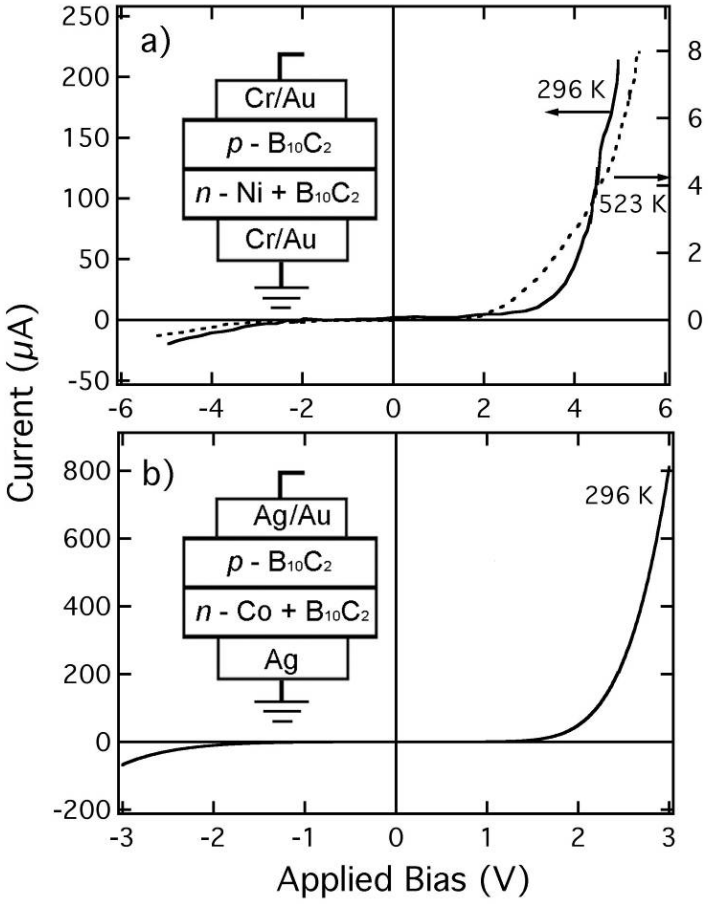

Figure 5-6. The diode I-V characteristics of a) Ni(*n*)-$B_{10}C_2$/(*p*)-$B_{10}C_2$ [1,10], and b) Co(*n*)-$B_{10}C_2$/(*p*)-$B_{10}C_2$, formed from the PECVD decomposition of orthocarborane (see text). The insets are schematics of the diodes, as assembled.

Ag substrates provided the best results as the increased surface roughness of the Ni and Al substrates often caused shorts through the thin film or very low currents (very high resistance) likely indicating incomplete film bonding to the metal surface. Sputtered Au with Ag epoxy and Cu wire contacts provided good ohmic contacts. The base film of

the diodes was fabricated using plasma enhanced chemical vapor deposition (PECVD) of a cobaltocene, orthocarborane and argon carrier gas mixture followed by a layer of PECVD decomposed orthocarborane using argon as a carrier gas. The growth parameters of the successful homojunction diodes are shown in Table 5-1.

Table 5-1. Plasma enhanced chemical vapor deposition (PECVD) growth parameters of successful Co doped diodes.

	Growth Time (min)	Cobaltocene Temperature (°C)	Cobaltocene Partial Pressure (mTorr)	Orthocarborane Temperature (°C)	Orthocarborane Partial Pressure (mTorr)	Argon Temperature (°C)	Argon Partial Pressure (mTorr)	Substrate Temperature (°C)
Base Film	**4.5**	**100**	**75**	**24**	**25**	**60**	**150**	**340**
Top Film	**12**	**N/A**	**N/A**	**60**	**50**	**60**	**150**	**340**

Similar to results found using nickeloene, the resulting homojunction involved the doping of a more p-type boron carbide (relative to the "$C_2B_{10}H_x$" boron carbide formed from metacarborane decomposition), formed by the PECVD of orthocarborane. [1,29] Based on the diode characteristics, the cobalt dopant introduced using cobaltocene in the PECVD process is an n-type dopant. Although semiconducting boron carbides grown from the decomposition of metacarborane and cobaltocene do appear to have increased carrier concentrations as seen in the resistivity results, there has not been a successful diode formed by PECVD of metacarborane yet when doping with cobaltocene.

These are compelling indications that cobaltocene decomposition introduces a dopant, in much the same way as has been seen for nickelocene decomposition in the

PECVD process with orthocarborane. [1,4,10,11] Both nickelocene and cobaltocene can be used to fabricate "$C_2B_{10}H_x$" boron carbide homojunctions.

The apparent doping of semiconducting "$C_2B_{10}H_x$" boron carbide films by cobalt, as cobaltocene, as p-type at low temperature (~200 K) and n-type at room temperature and above highlights that boron carbides may not obey the conventions and phenomenology of dopants of silicon and germanium. While speculative, it may be that electron carrier creation requires a larger activation than hole carriers, although many more electron carrier states may exist. In such a system, p-type carriers dominate at lower temperatures and n-type carriers dominate at higher temperatures. These experimental results and this model appear to be consistent with the speculations about trapping states proposed by Werheit and coworkers. [5]

6. Conclusions and Recommendations

6.1. Conclusions.

The goal of this research was to determine if cobalt, in the form of cobaltocene, doped boron carbide semiconducting films. While cobaltocene decomposition introduces a dopant, in much the same way as has been seen for nickelocene decomposition [1,4,10,11] the majority carrier has not been conclusively established, and it is not clear that cobaltocene introduces an unambiguous p or n type dopant, although diodes can be formed using cobaltocene as a dopant.

Fabrication of a p-n junction diode resulted from the plasma enhanced chemical vapor deposition (PECVD) of a combined layer of cobaltocene and orthocarborane, a p-type boron carbide polytype, followed by a layer of PECVD deposited orthocarborane. This indicates that at room temperature, cobalt appears to be an n-type dopant.

Photoemission spectroscopy and inverse photoemission spectroscopy (PES/IPES) studies at low temperature (~200 K) indicate that the cobalt adds acceptor states characteristic of p-type dopants. Warming the sample to room temperature and repeating PES/IPES shows the Fermi level shifts closer to the conduction band, indicating a more n-type semiconductor material. This shift in apparent doping type at different temperatures highlights that dopants of semiconducting "$C_2B_{10}H_x$" boron carbide may act differently than the more conventional silicon and germanium dopants and that a different doping model is needed.

It is possible that electron carrier creation requires a larger activation energy than hole carriers, although many more electron carrier states may exist. In such a system, p-type carriers dominate at lower temperatures and n-type carriers dominate at higher

temperatures. These experimental results and this model appear to be consistent with the speculations about trapping states proposed by Werheit and coworkers and should be studied further. [5]

6.2. Significance of the Research

The research and development of boron carbide semiconductors in general has potentially significant application to the fields of neutron detection and neutron direct power conversion due to the boron-neutron interactions shown in equations (1-1). The current state of special nuclear material (SNM) detection using gamma spectroscopy techniques is marginal at best and helps drive this current research into neutron detection methods that are likely to be significant improvements.

This research in particular is important to the future of these potential applications due to the continuing evolution of the understanding of boron carbide semiconducting film growth and doping characteristics. Besides finding another potential dopant that appears to have a catalytic effect on the rate of film growth, this research has potential applications in the field of spintronics as dilute magnetic semiconductors due to the ferromagnetic properties of cobalt.

The unexpected result of possible temperature dependence of doping type is significant in that the result had not been seen before and leads to additional studies that are necessary to more fully understand the properties of semiconducting boron carbide. It is now important to look at previously successful dopants to determine if they demonstrate the same temperature dependence and use these results to determine if the trapping state model proposed by Werheit, et al [5] is appropriate or if another model is

necessary. Another potentially significant result is the potential that this temperature dependence could lead to semiconductor applications that exploit this property. The apparent catalytic effect of introducing cobalt into the growing film is significant in that it may be possible to better control the film growth rate and material thickness properties by an appropriate level of doping. Industry would likely be interested in the 5-10 times quicker growth and associated use of a much smaller quantity of costly precursor material.

6.3. Recommendations for future research.

The following continuing research areas are important to assessing whether cobalt has practical applications when doping boron carbide:

Attempt to determine the majority carrier of cobalt doped boron carbide as a function of temperature using temperature dependent Hall Effect studies. Repeat the study using both metacarborane and orthocarborane to determine if doping is polytype dependent. This research could provide further information on any additional differences besides semiconductor type between the different boron carbide polytypes.

Repeat photoemission/inverse photoemission studies using cobaltocene doped orthocarborane to study possible polytype dependence of doping.

Attempt to fabricate a homojunction using cobaltocene doping of metacarborane to determine characteristics of a potential n-n+ junction. This research could determine if better diodes could be fabricated as n-n+ instead of p-n junctions.

Repeat photoemission/inverse photoemission studies and homojunction fabrication using cyclopentadienyl cobalt(I) dicarbonyl. This liquid cobalt compound should be studied to compare doping results to cobaltocene.

Attempt to fabricate thick cobaltocene fragment doped boron carbide homojunction films and compare neutron detection efficiency to previously tested thin heteroisomeric diodes. Vary the level of cobalt doping to determine the film growth rate dependence upon doping level.

Determine magnetic properties of cobalt-doped boron carbide using magneto-resistance studies as a preliminary result indicated anisotropic magnetoresistance. This research further explores the potential of cobalt doped boron carbide to act as a dilute magnetic semiconductor.

Appendix A. Detailed PECVD Procedure

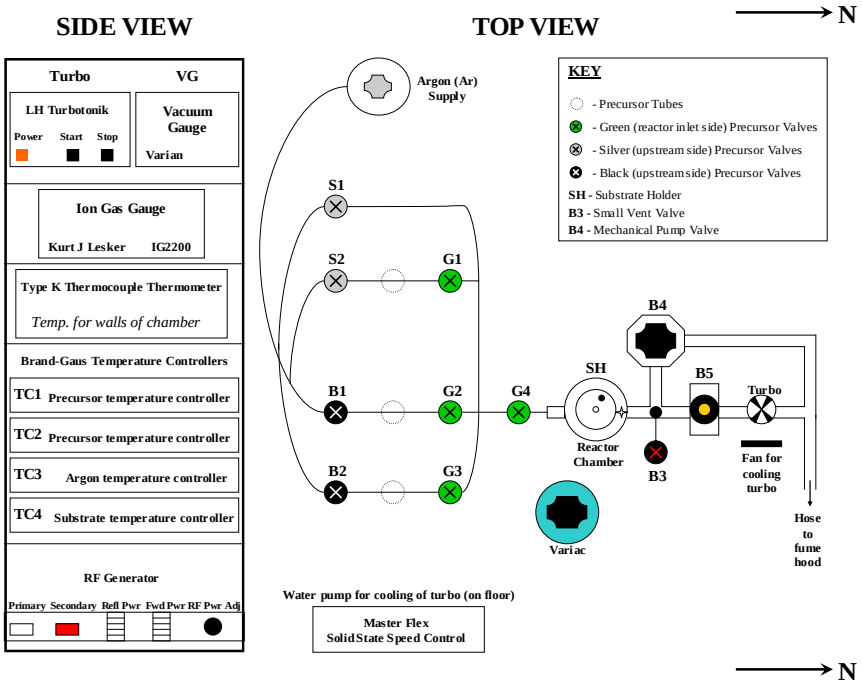

Figure A-1. Schematic of the plasma enhanced chemical vapor deposition (PECVD) system.

a. The normal configuration for the reactor when not in use is under vacuum such that valve (B4) is open and all other valves are closed. To bake out overnight, heat the argon supply line (TC3) to 102^{o}C to bake out and heat the reactor walls to 102^{o}C (~75 on the Variac). Argon tank valve should be closed and valves (S1) and (G4) open.

b. Turn on the RF primary power at least 15 minutes prior to creating a plasma so that the system is warmed up. Start preparing substrates as shown in 8.2.

c. To remove the substrate holder, close all valves and slowly open valve (B3). Monitor the vacuum gauge (VG); when gauge goes to “ATM”, the substrate holder can be removed.

d. Once the substrates are ready, clean the substrate holder, mask, and screws with Kimwipes and acetone/ethanol. Ultrasonic cleaning of the mask in ethanol or acetone may also be done. Dry all parts with the nitrogen gun.

e. Using clean tools and clean gloves, place the substrates on the substrate holder and tighten the mask with clean nuts and bolts. Tighten screws in a clockwise fashion to avoid warping of the mask.

f. Insert the substrate holder into the reactor's chamber and ensure the O-ring is not pinched. Orient the substrate holder so that the screw on top is pointing to the "north" in order to monitor growth rates as film thicknesses will vary. Install the cartridge heater and the thermocouple into the substrate holder.

g. Verify valve (B3) is closed and open (S1) and (G4). Allow vacuum pressure to fall as far as the mechanical pump (B4) will go.

h. Turn on argon temperature controller (TC3) to 60^{o}C.

i. Activate the turbo pump by pushing the "Start" button on the LH Turbotronik controller and turn on the accessory cooling fan. When the "NORM" light on the LH Turbotronik controller comes on, close the mechanical pump valve (B4) and open the turbo valve (B5).

j. Turn on the substrate temperature controller (TC4) and set to 340^{o}C for metal substrates or 345^{o}C for silicon substrates. To do this, on (TC4) press the "right" arrow key then press the "up" arrow key to adjust to desired temperature. To set the temperature, press the "right" arrow key.

k. After 10 minutes of pumping with the substrate up to the desired temperature, turn off the turbo by pushing “Stop” on the LH Turbotronik controller. Open the mechanical pump valve (B4) and close the turbo valve (B5).

l. Open the argon tank valves and set the pressure to about 200 mTorr by slowly opening and adjusting valve (S1). Continue purging for a minute or two after which the plasma should be struck by turning on the RF secondary power and setting the power adjustment knob to give only 1 LED glowing level on “FWD PWR” meter. Turn the power knob until two LEDs are glowing then return to one LED.

m. Begin heating precursors to desired temperature to ensure vaporization is at maximum before deposition.

n. Plasma etch for at least 20 minutes. After etching, stop the plasma and decrease the argon pressure to 150 mTorr.

o. With the plasma off, open the desired carborane precursor valves and regulate to the desired pressure by adding to the argon base pressure. Once stabilized, open the cobaltocene valves and regulate to the desired partial pressure. Once stabilized, restrike the plasma as discussed above and grow film for desired time.

p. NOTE: Always open precursor valves from right to left (e.g. G1 then S2) and close valves from left to right (e.g. B1 then G2) to minimize pressure spikes in the reactor.

q. For heterojunction films, close the precursor valves and stop the plasma after the desired growth time. Move to step “s”.

r. For homojunction films, close the precursor valves and stop the plasma. Flush the system with ~2000 mTorr of argon and then reset to 150mTorr. Once stabilized,

open the valves for the same carborane precursor used for the doped film and regulate to the desired partial pressure. Restrike the plasma and grow for the desired time.

s. To terminate the deposition process, close the precursor valves. Turn the RF power adjustment knob counterclockwise until it stops and switch off the RF power secondary switch. Flush with argon again using ~2000mTorr to help remove un-decomposed precursors. Let the RF generator run for at least 15 minutes before the RF primary power is switched off to allow proper cool down of the RF generator.

t. Close the Ar valves (S1 and tank valve) and the reactor's inlet valve (G4) if reactor cooling is desired to take place in vacuum. If oxygen contamination appears to be a problem, 200mTorr of argon during cooldown reduces the oxygen effect.

u. Switch off all temperature controllers and heaters except the substrate temperature controller (TC4).

v. Run the ramped cool down profile on the substrate temperature controller (TC4) by pressing the green button, push the "right" arrow key to select "yes" then use the "down" arrow key scroll to "Cool down" and then push the "right" arrow key to select this profile. The system will then cool slowly over ~3 hours.

Appendix B. Detailed Substrate Preparation Procedure.

a. Wear nitrile gloves when handling and cleaning substrates to avoid contamination.

b. Cut the substrates (metal, glass, silicon, etc) to the correct dimensions to fit the mask. Use a sharp object like a small screwdriver to label the metal or silicon type.

c. For metal substrates:

1. Place cut substrates into an acetone bath and place in ultrasonic cleaner for 10 minutes. Repeat in an ethanol bath for 10 minutes.

2. After ultrasonic cleaning, dry and place substrates on the substrate holder. (Return to PECVD Procedure as shown in appendix 8.1)

d. For silicon substrates:

1. Fill a 200 mL flask with ultra-pure water; purge the ultra-pure water with nitrogen gas for at least 20 minutes in order to deionize the water.

2. Place cut substrates into an acetone bath and place in ultrasonic cleaner for 10 minutes. Repeat in an ethanol bath for 10 minutes.

3. After ultrasonic cleaning, place substrates in a plastic dish of hydrofluoric acid (HF) in the fume hood with their glazed surfaces upright and etch for at least 10 minutes.

4. To handle HF: Wear glass shield, apron, nitrile gloves, glasses, etc. Ensure that you are not wearing any rings on your fingers, watches, contact lenses, or open-toed shoes.

5. Using plastic tweezers, place the substrates into the deionized water. (*no time limit required*)

6. Dry substrates with nitrogen gun and place on substrate holder.

Appendix C. Detailed contact fabrication procedures.

a. In order to minimize oxygen exposure to the films before adding contacts, conduct the following preparatory steps while the films are still under vacuum in the reactor.

1. Clean sputtering masks with acetone/ethanol and Kim Wipes and then dry with the nitrogen gun.

2. Ensure sputtering machine vacuum is sufficient (<10mTorr) and that the gold target is installed.

3. Strip the oxide off of 36 gauge bare copper wire using emery cloth and wipe off residue with a Kim Wipe. Cut enough wires, ~1/2" long, for the number of contacts needed for all films.

4. Stir the Epotex P1011S silver epoxy until smooth.

5. Begin heating oven to 80 ^{o}C.

b. Remove three films from reactor and return fourth film to reactor and vacuum as quickly as possible as sputtering machine can only do three films at a time.

c. Using gloves, quickly place the three films in the sputtering masks and place in sputtering dome. Several times during pump down, flush the system with argon using the "vent" valve. This eliminates air and allows a better vacuum which pulls down more quickly.

d. Once the vacuum is <10mTorr, increase the argon pressure to ~30mTorr.

e. If using metal substrates, ensure the three way electrical switch is in the sputtering, and not etching, position. If using silicon, cover the contact sputtering holes

with a clean microscope slide and use the “Plasma Etch” setting to etch a contact on the silicon for 10 minutes using the settings in (f) below. Remove the glass slide.

f. Turn on the voltage supply power and increase voltage slowly until 10mA is showing on the ammeter. The pressure will typically spike and have to be reduced while simultaneously increasing the voltage. Increase the voltage to 9V while decreasing the pressure and maintaining 10mA of current. Once stabilized, sputter for 10 minutes.

g. At the end of the sputtering time, turn off the vacuum pump and open the vent valve to break the dome seal. Remove the films using gloves or tweezers. Repeat the process above with the fourth film. Place the substrates on a 4” glass dish to stabilize wires during movement to oven.

h. After the fourth film is done sputtering, place a small dot of silver epoxy in the center of each gold contact using a toothpick or similar tool as well as on the metal substrate. If using a silicon substrate, use a deburring bit on the rotary tool to grind off the oxide and immediately place a drop of silver epoxy on the spot. Use tweezers to place a piece of wire on the silver epoxy. It is often necessary to bend a 90° angle at the very end of the wire to place in the epoxy to keep the silver from “walking” along the wire during baking and shorting to the substrate.

i. Place the substrates in the oven and bake at 80°C for 30 minutes. Turn the oven up to 150°C. Once the oven is up to temperature, bake for an additional 60 minutes to allow for full curing.

j. Turn the oven temperature controller down to less than room temperature and allow the substrates to cool down as slowly as possible by keeping the oven closed. Once

the temperature has dropped below about 30°C, the substrates can be removed for I-V curve testing.

k. Place each film in a plastic storage case and label the box with the growing procedures.

Appendix D. Homojunction Growth Parameters.

The growth parameters shown below are for the homojunction films grown after the resistivity and initial photoemission/inverse photoemission results. The unsuccessful growths on silicon are not listed as the partial pressure ratios and precursor temperatures used ensure that essentially no cobalt was doped into the films.

Table D-1. Growing parameters for homojunctions.

Set		Growth Time (min)	Cobaltocene Temperature (°C)	Cobaltocene Partial Pressure (mTorr)	Orthocarborane Temperature (°C)	Orthocarborane Partial Pressure (mTorr)	Argon Temperature (°C)	Argon Partial Pressure (mTorr)	Substrate Temperature (°C)	Results
1	Base Film	6	100	100	30	50	60	150	340	Very thick film (black) with linear, low (10^{-10}A) currents.
	Top Film	15	N/A	N/A	60	50	60	150	340	
2	Base Film	6	100	75	24	25	60	150	340	Film thinner than Set 1 but still very thick. Start to get shorts indicating base film too metallic and top film too thin.
	Top Film	10	N/A	N/A	60	50	60	150	340	
3	Base Film	5	100	53	24	35	60	150	340	Film slightly thinner than Set 2 – portions < 1um; I-V curves start to show symmetry about origin but low currents (10^{-8}A);
	Top Film	20	N/A	N/A	60	50	60	150	340	
4	Base Film	4.5	100	75	24	25	60	150	340	Junctions on Ag substrates at thinner portions of film (~400nm);
	Top Film	12	N/A	N/A	60	50	60	150	340	

References.

[1] S.-D. Hwang, K. Yang, P.A. Dowben, A.A. Ahmad, N.J. Ianno, J.Z. Li, J.Y. Lin, H.X. Jiang and D.N. McIlroy, *Appl. Phys. Lett*. **70**, 1028-1030 (1997).

[2] A.N. Caruso, P.A. Dowben, S. Balkir, Nathan Schemm, Kevin Osberg, R.W. Fairchild, Oscar Barrios Flores, Snjezana Balaz, A.D. Harken, B.W. Robertson and J.I. Brand, *Materials Science and Engineering* B **135** (2006), 129-133.

[3] A.N. Caruso, R.B. Billa, S. Balaz, J.I. Brand and P.A. Dowben, *J. Phys. Condensed Matter* **16**, L139-L146 (2004).

[4] D.N. McIlroy, S.-D. Hwang, K. Yang, N. Remmes, P.A. Dowben, A.A. Ahmad, N.J. Ianno, J.Z. Li, J.Y. Lin and H.X. Jiang, *Appl. Phys. A* **67,** 335-342 (1998).

[5] H. Werheit, R. Schmechel, V. Kueffel and T. Lundstrom, *J. Alloys and Compounds* **262**, 372-380 (1997).

[6] Sezer, J.I. Brand, *Materials Science and Engineering*, **B79** (2001), 191-202.

[7] T.L. Aselage, D. Emin, G.A. Samara, D.R. Tallant, S.B. Van Deusen, M.O. Eatough, H.L. Tardy, E.L. Venturini, *Physical Review B,* **48** (1993) 11759-11766.

[8] C.C. Ilie, S. Balaz, L.G. Rosa, J. Zhang, P. Lunca-Popa, C. Bianchetti, R. Tittsworth, J.I. Brand, B. Doudin, P.A. Dowben, *Applied Physics* A **81** (2005), 1613-1618.

[9] C.H. Liu, C. Huang, *Journal of Materials Science* **35** (2000) 387-390.

[10] S.-D. Hwang, N. Remmes, P.A. Dowben and D.N. McIlroy, *J. Vac. Sci. Technol. A* **15**, 854-859 (1997).

[11] S.-D. Hwang, N.B. Remmes, P.A. Dowben and D.N. McIlroy, *J. Vac. Sci. Technol. B* **14**, 2957-2960 (1996).

[12] http://mrsec.wisc.edu/Edetc/background/LED/band.htm.

[13] H.M. Rosenberg, The Solid State, Oxford Science Publications, Third Edition, 1995.

[14] www.public.asu.edu/~ntao1/ECE352/ECE05-1.ppt.

[15] Richard C. Jaeger, Travis N. Blalock, Microelectronic Circuit Design, McGraw-Hill, Second Edition, 2003.

[16] http://www.eecs.umich.edu/~singh/semi.html.

[17] James Petrosky, NENG660 Class Notes, 2006.

[18] http://www.phys.ntnu.no/~sraaen/dif4903/elspec.pdf.

[19] P. Lunca-Popa, J.I. Brand, S. Balaz, Luis G. Rosa, N.M. Boag, M. Bai, B.W. Robertson and P.A. Dowben, *J. Phys. D: Appl. Phys.* **38**, 1248-1252 (2005).

[20] http://www.sigmaaldrich.com/catalog/search/ProductDetail/ALDRICH/339164.

[21] L. Hernán, J. Morales, L. Sánchez, J. Santos, J.P. Espinós, A.R. González-Elipe, J.P. Holgado, *Surface Science* **477**, L295 (2001)

[22] C.A. Formstone, E.T. FitzGerald, P.A. Cox, and D. O'Hare, *Inorg. Chem.* **29**, 3860 (1990)

[23] J. Choi and P.A. Dowben, *Surface Science* **600** (2006), 2997-3002.

[24] O. Henrion, and W. Jaegermann, *Surface Sci*. **387**, L1073 (1997).

[25] C.H. Liu, *Materials Letters* **49** (2001), 308.

[26] F. Reinert, S. Hüfner, *New Journal of Physics* **7**, (2005) 97.

[27] P. W. Erdman and E. Zipf, C. *Rev. Sci. Instum.* **53**, 225-227 (1982).

[28] K. Shukla, S. Banik, S.R. Barman, *Current Science* **90(4)** (2006).

[29] Snjezana Balaz, Dimtcho I. Dimov, N.M. Boag, Kyle Nelson, Benjamin Montag, J.I. Brand, and P.A. Dowben, *Appl. Phys. A* **84** (2006), 149-159.

[30] D. Briggs, M.P. Seah, Practical Surface Analysis, John Wiley & Sons. Vol. 1, Second Edition (1993).

[31] M.G. Cook, N.S. Mcintyre, *Analytical Chemistry* **47**, 2208-2213 (1975).

[32] T.L. Barr, *J. Physical Chemistry* **82**, 1801-1810 (1978).

[33] Dongqi Li, P.A. Dowben, J.E. Ortega, and F.J. Himpsel, *Phys. Rev.* B **49** (1994), 7734–7738.

[34] P.A. Dowben, *Surface Science Reports* **40** (6-8) (2000), 151-247.

[35] J. E. Demuth, W.J. Thompson, N.J. DiNardo and R. Imbihl, *Phys. Rev. Lett.* **56**, 1408-1411 (1986).

[36] K. Stiles and A. Kahn, *Phys. Rev. Lett.* **60**, 440-443 (1988).

[37] D. Yao, and B. Kim, *Applied Thermal Engineering* **23**, 341 (2003).

[38] B.W. Robertson, S. Adenwalla, A. Harken, P. Welsch, J.I. Brand, P.A. Dowben and J.P. Claassen, *Appl. Phys. Lett.* **80**, 3644-3646 (2002).

[39] B.W.Robertson, S. Adenwalla, A. Harken,, P. Welsch, J.I. Brand, J.P. Claassen, N. .M. Boag and P.A.Dowben, in *Advances in Neutron Scattering Instrumentation*, ed. I.S. Anderson, B. Guérard, *Proc. SPIE* **4785**, 226-233 (2002).

[40] S. Adenwalla, R. Billa, J.I. Brand, E. Day, M.J. Diaz, A. Harken, A. McMullen-Gunn, R. Padmanabhan and B.W. Robertson, in: *Penetrating Radiation Systems and Applications V, Proc. SPIE* **5199**, 70-74 (2003).

[41] A.D. Harken, E.E. Day, B.W. Robertson and S. Adenwalla, *Jap. J. Appl. Phys.* **44**, 444-445 (2005).

[42] K. Osberg, N. Schemm, S. Balkir, J.I. Brand, S. Hallbeck, P. Dowben and M.W. Hoffman, *IEEE Sensors Journal* **6** (2006), 1531-1538.

[43] H. Takizawa, N. Haze, K. Okamoto, K. Uheda and T. Endo, *Materials Research Bulletin* **37**, 113-121 (2002).

[44] U. Kuhlmann, H. Werheit, J. Pelloth, W. Keune and T. Lundstrom, *Physica Status Solidi B- Basic Research* **187**, 43-59 (1995).

[45] U. Kuhlmann, H. Werheit, T. Dose and T. Lundstrom, *J. Alloys and Compounds* **186**, 187-200 (1992).

[46] A.N. Caruso, Snjezana Balaz, Bo Xu, P.A. Dowben, A.S. McMullen-Gunn, J.I. Brand, Y.B. Losovyj, D.N. McIlroy, *Applied Physics Letters* **84** (2004) 1302-1304.

[47] D.N. McIlroy, C. Waldfried, T. McAvoy, Jaewu Choi, P.A. Dowben and D. Heskett, *Chem. Phys. Lett.* **264** (1997) 168-173.

[48] D.N. McIlroy, J. Zhang, P.A. Dowben and D. Heskett, *Mat. Sci. Eng.* A **217/218** (1996), 64-68.

[49] D.N. McIlroy, Jiandi Zhang, P.A. Dowben, P. Xu and D. Heskett, *Surface Science* **328** (1995), 47-57.

[50] A.N. Caruso, L. Bernard, B Xu and P.A.Dowben, *J. Phys. Chem. B* **1079**, 9620-9623 (2003).

[51] H. Zeng, D. Byun, J. Zhang, G. Vidali, M. Onellion and P. A. Dowben, *Surf. Sci.* **313**, 239-250 (1994).

[52] J. Zhang, D.N. McIlroy, P.A. Dowben, Hong Zeng, G. Vidali, D. Heskett and M. Onellion, *J. Phys. Cond. Matt.* **7,** (1995) 7185-7194.

[53] M. Alonso, R. Cimino and K. Horn, *Phys. Rev. Lett.* **64**, 1947-1950 (1990).

[54] B Sadigh, T.J. Lenosky, M.-J. Caturla, A.A. Quong, M. M. Giles, M. Foad, C.D. Spataru and S.G. Louie, *Applied Physics Letters* **80**, 4738 (2002).

[55] Sunwoo Lee, J. Mazurowski, G. Ramseyer, and P.A. Dowben, *Journ. Appl. Phys.* **72** (1992), 4925–4933.

REPORT DOCUMENTATION PAGE

Form Approved
OMB No. 074-0188

1. REPORT DATE *(DD-MM-YYYY)*	**2. REPORT TYPE**	**3. DATES COVERED** *(From – To)*
26-02-2007	**Master's Thesis**	Jun 2006 – Mar 2007

4. TITLE AND SUBTITLE

Cobalt Doping of Semiconducting Boron Carbide Using Cobaltocene

5a. CONTRACT NUMBER

5b. GRANT NUMBER

5c. PROGRAM ELEMENT NUMBER

6. AUTHOR(S)

Carlson, Lonnie, Major, USA

5d. PROJECT NUMBER
2006-073

5e. TASK NUMBER

5f. WORK UNIT NUMBER

7. PERFORMING ORGANIZATION NAMES(S) AND ADDRESS(S)
Air Force Institute of Technology
Graduate School of Engineering and Management (AFIT/EN)
2950 Hobson Way
WPAFB OH 45433-7765

8. PERFORMING ORGANIZATION REPORT NUMBER

AFIT/GNE/ENP/07-01

9. SPONSORING/MONITORING AGENCY NAME(S) AND ADDRESS(ES)
DTRA/CSNS
Attn: Geraldine Bright
8725 John J. King Blvd
Ft Belvoir, VA 22060-6201 703-767-4474 DSN 427-4474

10. SPONSOR/MONITOR'S ACRONYM(S)

11. SPONSOR/MONITOR'S REPORT NUMBER(S)

12. DISTRIBUTION/AVAILABILITY STATEMENT
APPROVED FOR PUBLIC RELEASE; DISTRIBUTION UNLIMITED.

13. SUPPLEMENTARY NOTES

14. ABSTRACT

The decomposition of cobaltocene and metacarborane (*closo*-1,7-dicarba-decaborane) under low energy electron irradiation at about 200 K results in a material with the Fermi level closer to the valence band than the material resulting from the decomposition of metacarborane alone. This indicates that cobaltocene provides a relatively p-type dopant as seen in ultraviolet photoemission spectroscopy/inverse photoemission spectroscopy. Upon warming to room temperature, however, the Fermi level shifts towards the conduction band, suggesting an n-type dopant. This temperature dependent surface photovoltage effect is not compelling evidence for the majority carrier type but does suggest an increase in the carrier concentration in semiconducting boron carbides with cobaltocene fragment doping.

Using cobaltocene to introduce dopants into a orthocarborane (*closo*-1,2-dicarbadecaborane) derived film, deposited by plasma enhanced chemical vapor deposition, a semiconducting boron carbide homojunction diode has been fabricated. This diode has potential applications in neutron detection, direct neutron power conversion, and as a dilute magnetic semiconductor.

15. SUBJECT TERMS
Boron Carbides; Semiconductor Devices; Cobalt; Doping; Chemical Vapor Deposition; Neutron Detectors;

16. SECURITY CLASSIFICATION OF:			**17. LIMITATION OF ABSTRACT**	**18. NUMBER OF PAGES**	**19a. NAME OF RESPONSIBLE PERSON**
REPORT	**ABSTRACT**	**c. THIS PAGE**			David LaGraffe, LTC, USA (ENP)
U	**U**	**U**	**UU**	100	**19b. TELEPHONE NUMBER** *(Include area code)* (937) 255-3636, ext 7308; e-mail: David.LaGraffe@afit.edu

Standard Form 298 (Rev: 8-98)
Prescribed by ANSI Std. Z39-18